Considering Electrocatalytic Ammonia Synthesis via Bimetallic Dinitrogen Cleavage

Quinton J. Bruch,[1,‡] Gannon P. Connor,[2,‡] Noah D. McMillion,[1,‡] Alan S. Goldman,[3] Faraj Hasanayn,[4,*] Patrick L. Holland,[2,*] and Alexander J. M. Miller[1,*]

[1] Department of Chemistry, University of North Carolina at Chapel Hill, Chapel Hill, North Carolina 27599-3290, United States

[2] Department of Chemistry, Yale University, New Haven, Connecticut 06520, United States

[3] Department of Chemistry and Chemical Biology, Rutgers, The State University of New Jersey, New Brunswick, New Jersey 08903, United States

[4] Department of Chemistry, American University of Beirut, Beirut 1107 2020, Lebanon

‡ These co-authors contributed equally.

Corresponding Authors:

*E-mail: fh19@aub.edu.lb (F.H.)

*E-mail: patrick.holland@yale.edu (P.L.H.)

*E-mail: ajmm@email.unc.edu (A.J.M.M.)

Abstract. Despite advances in the development of molecular catalysts capable of reducing dinitrogen to ammonia using proton donors and chemical reductants, few molecular electrocatalysts have been discovered. This Perspective considers the prospects of electrocatalyst development based on a mechanism featuring the cleavage of N_2 into metal nitride complexes. By understanding the factors that control the reactivity of individual steps along the electrochemical N_2 cleavage path, opportunities for new advances are identified. Ligand design principles for facile electrochemical N_2 binding, formation of bridging N_2 complexes, thermal or photochemical N_2 cleavage, and conversion of a nitride ligand into ammonia are described, featuring recent advances and the authors' collaborative work on rhenium complexes.

Keywords. Nitrogen, Ammonia, Electrocatalysis, Electrochemistry, Dinitrogen Cleavage

TOC Graphic.

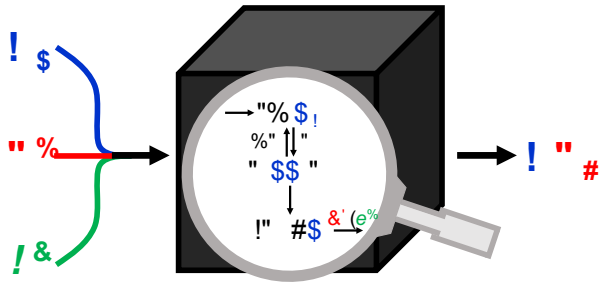

1. Introduction

The sustainable use of atmospheric N_2 in chemical transformations represents a scientific challenge with the potential for great societal impact. Fixation of atmospheric N_2 into ammonia is crucial in agriculture and human nutrition, and is also important for the synthesis of commodity chemicals.[1,2] This Perspective explores a particular electrochemical approach to nitrogen fixation and ammonia electrosynthesis, using molecular catalysts that cleave N_2 into two metal nitride complexes, $L_nM{\equiv}N$. We examine the key steps in this bimetallic electrochemical N_2 cleavage mechanism and describe emerging design principles.

The primary industrial method currently used to reduce N_2 to NH_3 is the high-temperature and high-pressure Haber-Bosch process (HB), which uses H_2 as the source of protons and electrons. The catalysts and methods were first discovered by Haber, for which he was awarded the Nobel Prize in Chemistry in 1918. Bosch was then awarded the 1931 Nobel Prize for development of the high pressure methods required to bring the Haber catalysis to practical fruition. The impact of HB on humankind is difficult to overstate: the large-scale synthesis of fertilizer has dramatically increased food production, supporting a growing global population. The impact has been summed up by Smil: without HB, almost two-fifths of the world's population would not be here, because there would not be enough food for them to eat.[3] Study of HB methods and catalysts has also stimulated advances in fundamental chemistry, highlighted, for example, by the Nobel Prize given to Ertl in 2007 for his elucidation of reactivity on surfaces.[4–6]

The H_2 used in HB is generally obtained through steam reforming of non-renewable fossil fuels. Indeed, the overall process of converting hydrocarbons, water, and nitrogen to ammonia currently consumes *ca*. 2% of global fossil fuel energy and produces commensurately large

amounts of CO_2.[7,8] Efforts to replace fossils fuels with renewable energy sources has challenged chemists to reimagine nitrogen fixation methods. Importantly, methods that could operate close to ambient temperatures and use renewable electrical energy would be much more environmentally friendly than HB (for more detail, see below).

There are additional advantages of moving beyond the HB process for nitrogen fixation. The high temperatures and pressures of HB lead to high capital costs and require a large scale to be economical.[9] Current ammonia production is therefore centralized, which can lead to high transportation costs.[10] In contrast, electrochemical processes can employ solar or wind energy, which is widely distributed, and can operate on a smaller scale, requiring less investment in infrastructure. It could therefore be possible to decentralize N_2 fixation with a method that could utilize renewable electricity and mild reaction conditions. This is advantageous because fertilizer could be produced from sun, air, and water at or near the fields where it is needed, reducing transportation costs. Thus, replacing the current HB method with an electrochemical alternative is a grand challenge in catalysis with the potential for widespread benefit to society.

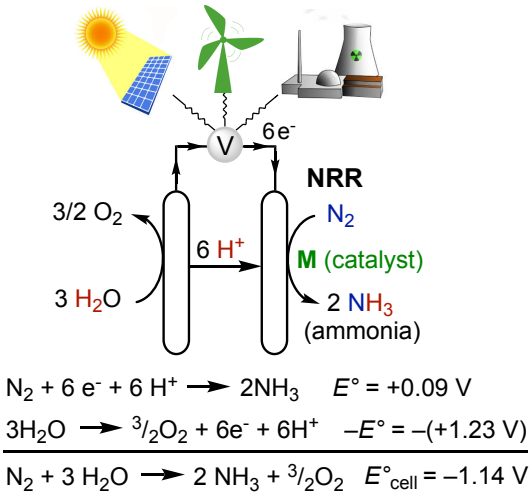

Figure 1. Schematic representation of sustainable ammonia electrosynthesis and corresponding half- and full-cell reactions with aqueous standard reduction potentials *vs* the normal hydrogen electrode (NHE) at standard state (1 atm N_2 and O_2, 1 M NH_3, pH 0, 298 K).[11]

The electrochemical nitrogen reduction reaction (NRR) is the half-reaction that converts N_2 into ammonia (Figure 1). The reduction of N_2 by electron/proton pairs has a standard reduction potential similar to the reduction of H^+ to H_2 in water.[12] For large-scale impact, the only feasible

source of protons and electrons is water. The standard cell potential for the overall aqueous electrochemical process in Figure 1 is E^{o}_{cell} = –1.14 V *vs* NHE (ΔG^{o} = +79 kcal/mol per mole of ammonia), and we have derived values in acetonitrile as well.[12] This indicates the need for a substantial input of energy. The ideal version of NRR would utilize electrochemical energy from renewable power, H atoms from water, and catalysts that operate near ambient temperature and pressure (Figure 1).[13–17]

We recently reported a detailed technoeconomic analysis designed to gauge whether an NRR system with water oxidation could be cost-effective on a large scale.[18] Currently, ammonia from HB is inexpensive because of the low price of the natural gas feedstock.[15,19,20] However, when even conservative literature estimates of the social cost of CO_2 emissions are considered,[21,22] the conventional HB route is more costly than a hypothetical NRR/water oxidation system with a Faradaic efficiency of 95% and 0.6 V cell overpotential. Thus, NRR can indeed provide an economic alternative — but only if these aspirational catalyst performance metrics can be approached through chemical and engineering research advances.

One inspiration for catalyst development comes from the multimetallic FeS clusters of nitrogenase enzymes that reduce N_2 using H^+ (from water), e^- (delivered at ca. –0.4 V *vs* NHE), and energy from the hydrolysis of 2 ATP per e^-.[23–25] Electrochemical catalysts capable of N_2 reduction to NH_3 using H^+ and e^- equivalents and sustainable electricity would be the most direct synthetic analogue to nitrogenase.

The discovery of active electrocatalysts for N_2 reduction has been extremely rapid over the last few years, and has been dominated by heterogeneous catalysts.[26] These have a wide variety of chemical compositions including Bi, Au, Mo, and other metals, and are still in the exploratory stage.[27–44] In a particularly good recent example, electrolysis catalyzed by molybdenum carbide nanorods on a glassy carbon electrode with 0.1 M aqueous HCl produced up to 95 micrograms of NH_3 per hour per milligram of catalyst, with a Faradaic efficiency of 8.1% and a current density of ~25 mA/cm^2 at –0.30 V vs RHE.[45]

There have also been important recent advances in molecular catalysts for N_2 fixation. Building on seminal early work of the groups of Pickett, Efimov, and Shilov (among others),[46–49] several exciting stoichiometric examples of electrochemical reduction of N_2 to NH_3 have appeared.[17] To date, however, we are aware of only one molecular catalyst for *electrocatalytic* ammonia production from N_2. Peters *et al.* used the iron catalyst shown in Figure 2 under 1 atm

N_2 in Et_2O solution at –35 ºC to generate up to 5.5 equiv NH_3 per metal center with up to 28% Faradaic efficiency.[50] The competition between proton reduction to produce H_2 versus N_2 reduction to produce NH_3 has significantly limited the efficiency of both molecular and materials electrocatalysts.

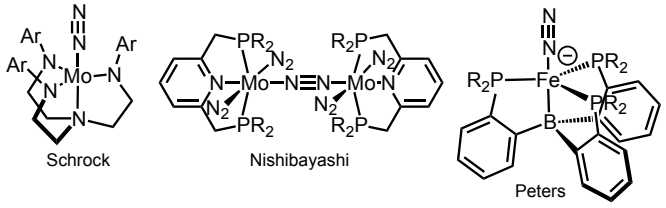

Figure 2. Molecular catalysts for N_2 reduction with acids and chemical reductants.

Molecular systems are amenable to detailed mechanistic study that can lead to deep insights and systematic improvements. Most mechanistic studies have utilized chemical reductants to drive the reactions, consistent with the conditions of most molecular catalysis.[51] Typically, transition metals (especially Fe and Mo) are used to activate N_2,[52–55] though there are recent advances using Lewis acids from group 13[56–58] and rare-earth elements.[59–63] Several mechanisms for stoichiometric and catalytic N_2 reduction using proton/electron equivalents have emerged from these studies. Current evidence supports an "alternating" path for N_2 reduction at the nitrogenase cofactor, with $1H^+/1e^-$ additions to the distal and proximal nitrogen atoms in turn (Scheme 1, purple arrows).[64–67] Ashley and coworkers reported a rare example of a molecular catalyst that follows the alternating pathway.[68] Chatt envisioned a distinct "distal" mechanism more than forty years ago (Scheme 1, blue arrows),[69,70] with initial $1H^+/1e^-$ additions only to the distal N. Chemical catalysis via this pathway was realized in 2003 by Yandulov and Schrock.[71,72] Recent discoveries by the groups of Nishibayashi[73–78] and Peters[79–81] have expanded the scope of Mo and Fe catalysts (for leading examples see Figure 2).

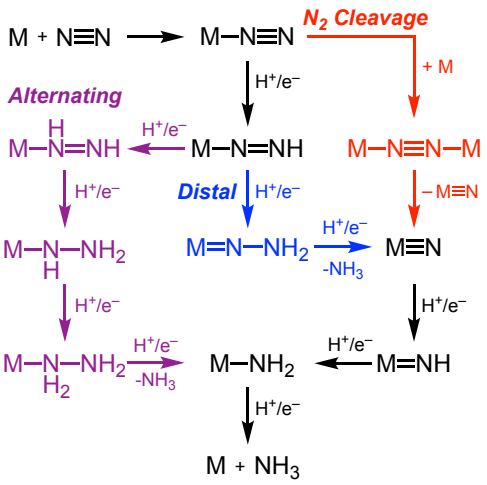

Scheme 1. Mechanistic pathways of N_2 reduction to NH_3.

This Perspective discusses a different mechanism: the N_2 cleavage path shown in red in Scheme 1. This pathway hinges on bimetallic N_2 cleavage to give two metal nitride complexes, a reaction that was first discovered by Cummins with Mo^{III} precursors.[82] Examples of N_2 cleavage to give bridging[83–90] and terminal[91–98] nitrides have since been reported.[99] Although N_2 cleavage still remains relatively rare, this mechanism could be advantageous because it avoids high-energy diazenido and hydrazido intermediates that lie on the distal pathway. In fact, the N_2 cleavage pathway is proposed in the molecular N_2 reduction catalysts with the highest turnovers reported so far.[94,97,100,101]

We focus here on research aimed at understanding the individual steps along the electrochemical N_2 cleavage path: electrochemically induced N_2 binding, thermal or photochemical N_2 cleavage, and conversion of nitride into ammonia. Applications of proton-coupled electron transfer (PCET) for the release of ammonia by breaking the metal-nitrogen triple bonds in intransigent nitride complexes are also described. We highlight examples from our collaborative studies of Re and Mo complexes capable of electrochemical N_2 cleavage to terminal metal nitrides and further reduction to give NH_3. Each section holds lessons that may guide the design of mechanistically well-defined NRR catalysts.

2. Electrochemically Induced N_2 Binding

Each dinitrogen reduction pathway of Scheme 1 involves N_2 coordination to a transition-metal center. The reactions are typically initiated by reduction of the metal center, and often dissociation of a ligand, which provide the metal center with an appropriate electronic structure for N_2 binding. Electrochemical methods, particularly cyclic voltammetry (CV), can elucidate mechanisms of N_2 binding.[102,103] Crucial electrochemical methods are highlighted in individual examples below. All potentials are reported in V vs the ferrocenium/ferrocene (Fc^+/Fc) reference,[104,105] unless noted otherwise.

2.1. Formation of Terminal N_2 Species.

In this section, we present reactivity trends that have emerged from electrochemical studies of transition metal complexes that bind N_2 as a terminal ligand upon a change in redox state. Terminally bound N_2 complexes represent likely intermediates leading to N_2-bridged dinuclear complexes along the path to N_2 cleavage. A key distinction is drawn between the case where reduction triggers a ligand substitution (with N_2 replacing a ligand on the complex) and the case where reduction is followed directly by N_2 association.

2.1.1. Electrochemically Induced N_2 Binding via Ligand Substitution. In one of the first reports of reductively triggered terminal N_2 binding, Pickett *et al.* studied the electrochemical conversion of *trans*-$Mo(dppe)_2(Cl)_2$ to *trans*-$Mo(dppe)_2(N_2)_2$ (Figure 3).[106,107] We present this study in detail as a prime example of the mechanistic insight that can be derived from cyclic voltammetry. The first reduction, from Mo^{II} to Mo^{I}, became reversible at higher scan rates, consistent with an electrochemical step followed by a chemical step, or EC process. A comparison of voltammograms under Ar and N_2 (Figure 3B) reveals distinct features, often an indicator of electrochemically induced reactivity with N_2. Comparing the CVs as a function of N_2 concentration indicated a dissociative mechanism involving reductively triggered chloride loss (Figure 3C), as distinguished from other possible EC pathways such as an associative ligand binding process or chemical redox disproportionation process. By estimating the upper limit of the rate for disproportionation of Mo^{I}, the latter pathway could be excluded since the rate constant for *trans*-$Mo(dppe)_2(N_2)_2$ formation using this equilibrium constant would be impossibly high. After initial Cl^- loss, one molecule of N_2 binds in the open coordination site. It was hypothesized that another reductive chloride dissociation (EC process) occurs next, followed by association of a second dinitrogen molecule to produce the ultimate product, *trans*-$Mo(N_2)_2(dppe)_2$. Th EC-type

mechanism exhibited by the Mo system is one of the most common pathways for electrochemically induced N_2 binding. The half-wave potential ($E_{1/2}$) in the halide series *trans*-Mo(X)$_2$(dppe)$_2$ (X = Cl, Br, I) shifts anodically (to less negative potentials) moving to heavier halides (Figure 3A), with each complex producing *trans*-Mo(N$_2$)$_2$(dppe)$_2$.[106,107] The cyanide complex *trans*-Mo(CN)(Cl)(dppe)$_2$ is even easier to reduce, but highlights limitations in electronic tuning: reduction generates *trans*-[Mo(CN)(Cl)(dppe)$_2$]$^-$, which does not readily lose chloride; despite moving to a less electron-rich complex, N_2 binding only occurs upon a second reduction at very negative potentials (–2.57 V).

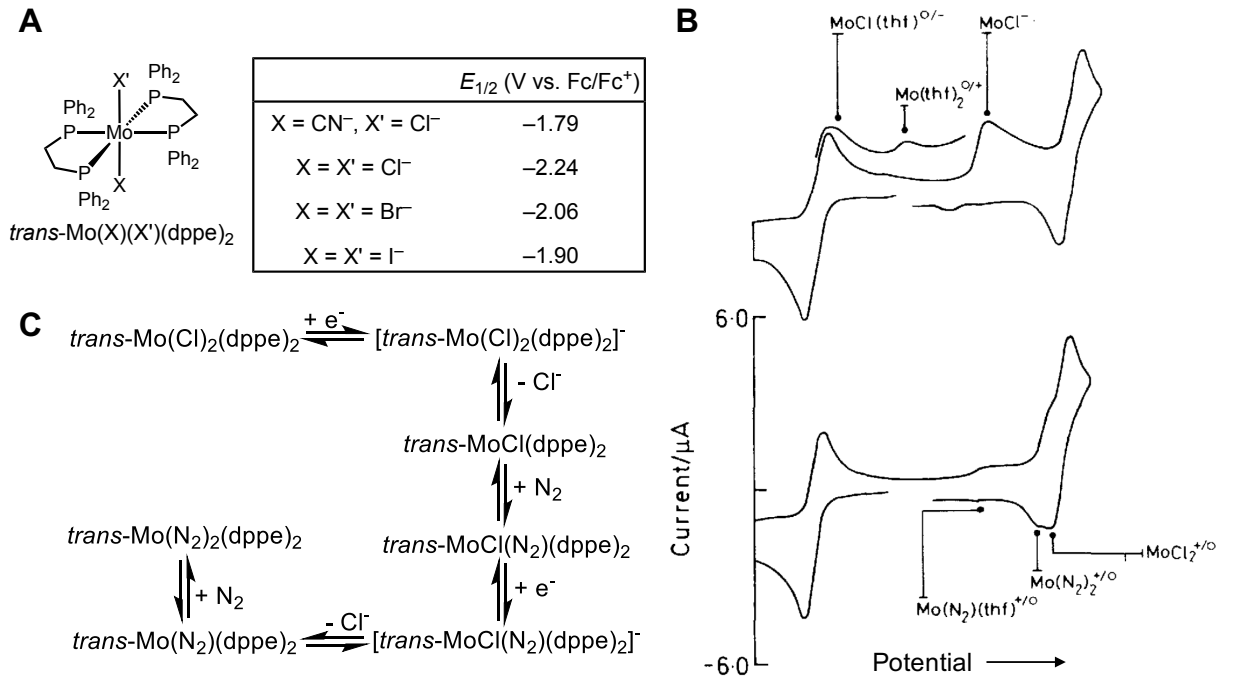

Figure 3. (A) Trends in reductive N_2 binding by Mo(X)(X')(dppe)$_2$ complexes. (B) Voltammograms of *trans*-Mo(Cl)$_2$(dppe)$_2$ in THF containing [Bu$_4$N][BF$_4$] under Ar (top) and N_2 (bottom), reproduced from reference [106] with permission of The Royal Society of Chemistry. (C) Proposed mechanism of N_2 binding by *trans*-Mo(Cl)$_2$(dppe)$_2$.[106]

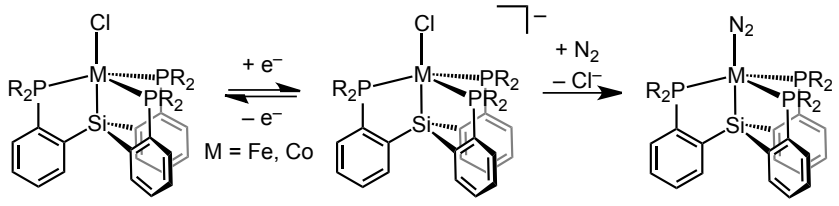

Figure 4. Reductive N_2 binding by tris(phosphino)silyl-supported iron and cobalt chloride complexes.[108]

Tripodal ligands constitute another rich platform for studies of N_2 binding (Figure 4). Peters *et al.* carried out a comparative study of tris(phosphino)silyl iron and cobalt chloride complexes with the formula $(SiP^R_3)MCl$ (Figure 4) examining their electrochemical reduction to give terminal dinitrogen complexes $(SiP^R_3)M(N_2)$ (M = Fe, Co; R = ^{i}Pr, Ph).[108] The Fe complex with R = ^{i}Pr and both Co complexes showed CVs with a reversible reduction under Ar. Under N_2, the reduction became irreversible and new features attributed to the dinitrogen complexes $(SiP^R_3)M(N_2)$ appeared.[109] This scenario is consistent with an associative mechanism in which N_2 binding assists with Cl^- dissociation, although a complete mechanistic study was not conducted. The reduction of $(SiP^R_3)FeCl$ (R = Ph) was reversible under both Ar and N_2, suggesting that N_2 does not bind on the timescale of the experiment.

The studies on reductive ligand substitution with N_2 provide a number of insights. For the supporting ligands, it is essential to provide sufficient electron density to promote ligand loss and N_2 binding while retaining an electrochemically accessible reduction. The nature of the dissociating ligand is particularly important in controlling both the reduction potential and substitution kinetics related to the N_2 binding process. For example, complexes of heavier halides were found to be easier to reduce and undergo more rapid halide ion dissociation in one system.[106] Solvent choice can also play a key role, especially since solvent coordination may occur upon halide dissociation, necessitating subsequent displacement of the solvent by N_2.[106]

2.1.2. Electrochemically Induced N_2 Association. Systems that bind N_2 upon reduction without requiring dissociation of another ligand are particularly interesting because they can circumvent any kinetic limitations imparted by an additional ligand dissociation step.

Peters *et al.* showed that the cationic complex with a vacant site (or weakly bound solvent) *trans* to boron $[(TPB)Fe]^+$ (Figure 5A) is an electrocatalyst for N_2 reduction to NH_3.[50,79,110,111] Electrochemical reduction ($E_{1/2}$ = –1.5 V) induces N_2 binding to yield the neutral dinitrogen complex $(TPB)Fe(N_2)$ (Figure 5A).[112] Electrochemically induced N_2 binding was also examined in a series of heterobimetallic cobalt complexes by Lu *et al.* (Figure 5B).[113] The complexes with more negative reduction potentials exhibited a greater degree of N_2 activation, attributed to the electronegativity of the metal *trans* to N_2.[113] A CE mechanism consisting of a chemical step (N_2 binding) followed by an electrochemical step ($1e^-$ reduction) was also observed during reductive N_2 binding by tris(anilido)molybdenum(III) complexes, for which an electrochemical response is

only observed under an N_2 atmosphere.[114] To our knowledge, kinetic studies of N_2 association were not conducted for these systems.

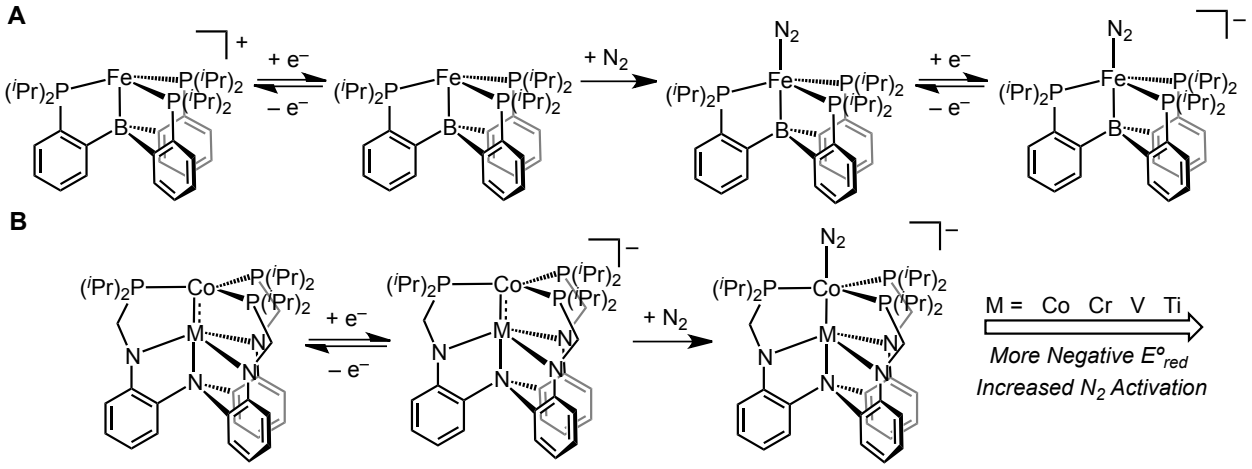

Figure 5. (A) Reductive N_2 binding by $[(TPB)Fe]^+$, which features an axial vacant site.[112] (B) Reductive N_2 binding by heterobimetallic cobalt complexes featuring axial vacant sites.[113]

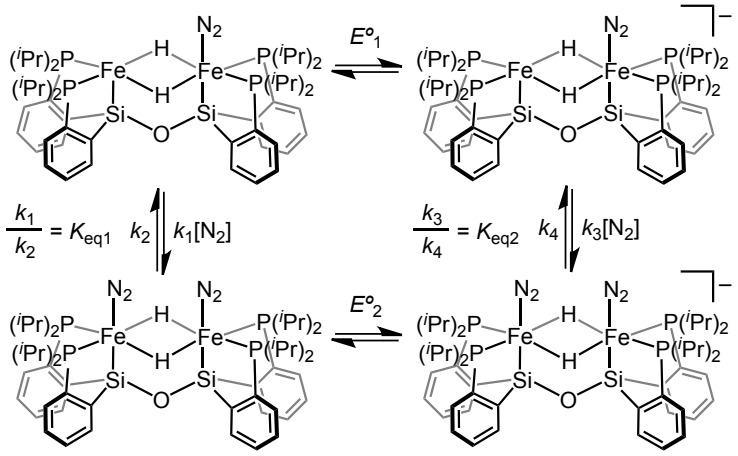

Parameters	Simulated Values
$E°_1$ (V)	–2.40
$E°_2$ (V)	–2.02
K_{eq1} (M^{-1})	1.1 (fixed)
K_{eq2} (M^{-1})	2.86 x 10^6
k_1 (M^{-1} s^{-1})	5.20 x 10^5
k_3 (M^{-1} s^{-1})	7.06 x 10^8

Figure 6. Thermodynamic and kinetic analysis of reductive N_2 association in a diiron system.[115]

Mechanistic studies of coordinatively unsaturated systems can probe the kinetics and thermodynamics of reductive N_2 association directly, since there are no competing ligand dissociation steps. For example, Peters *et al.* studied the binding of a second N_2 molecule to a homobimetallic diiron complex upon reduction,[115] gathering evidence in CV studies for the involvement of two competing mechanisms (Figure 6). At slow scan rates, a CE mechanism is dominant. N_2 binds to the Fe^{II}/Fe^{II} state in an unfavorable equilibrium, and the small equilibrium population of the bis(dinitrogen) complex is readily reduced due to the π-acidic N_2 ligand. At faster scan rates, electrochemical reduction outcompetes N_2 binding to the Fe^{II}/Fe^{II} state, resulting in an EC mechanism in which reduction occurs prior to N_2 binding. Initial reduction of the mono(dinitrogen) Fe^{II}/Fe^{II} complex occurs at more negative potentials, followed by strong N_2 binding. The binding affinity for N_2 by the Fe^{II}/Fe^{I} state is 10^6 times greater than that of the Fe^{II}/Fe^{II} state.[115]

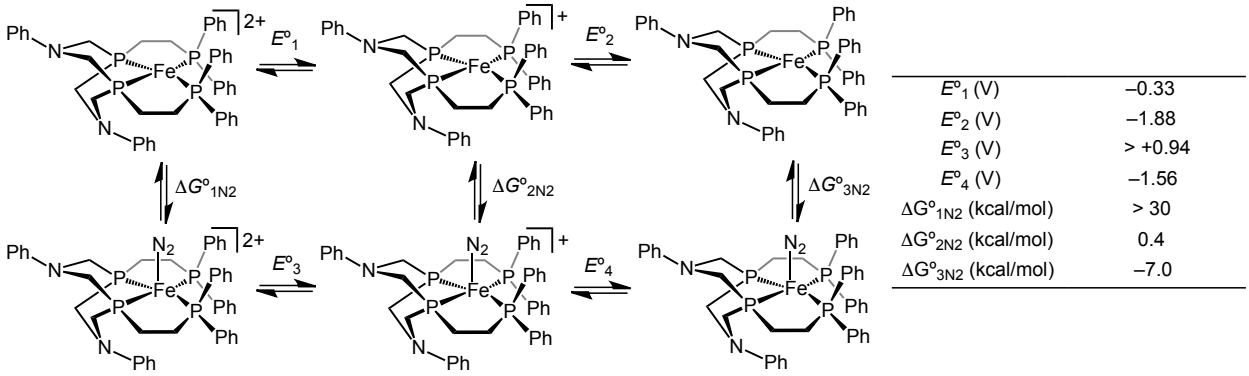

$E°_1$ (V)	–0.33
$E°_2$ (V)	–1.88
$E°_3$ (V)	> +0.94
$E°_4$ (V)	–1.56
$\Delta G°_{1N2}$ (kcal/mol)	> 30
$\Delta G°_{2N2}$ (kcal/mol)	0.4
$\Delta G°_{3N2}$ (kcal/mol)	–7.0

Figure 7. Thermodynamic analysis of reductive N_2 binding by an iron tetraphosphine complex.[116]

Redox-state-dependent N_2 binding was also examined by Mock *et al.* in Fe complexes supported by a macrocyclic tetraphosphine ligand (Figure 7).[116] Spectroelectrochemical studies enabled the construction of a thermochemical cycle (Figure 7). In this system, N_2 binding to the Fe^{II} complex is endergonic by more than 30 kcal/mol, binding to Fe^{I} is ergoneutral ($\Delta G°$ = 0.4 kcal/mol), and N_2 binding to Fe^0 is exergonic (–7.0 kcal/mol). This represents an increase in binding affinity of as much as 10^{22} upon reduction from Fe^{II} to Fe^0.

Overall, complexes with an available N_2 binding site in their oxidized form can bind N_2 either before reduction (CE mechanism) or after reduction (EC mechanism). The ability to bind N_2 in the oxidized form has been valuable for enabling quantification of the redox-state-dependent

N_2 binding affinity. A large increase in N_2 binding affinity is typically observed upon reduction, due to increased π-backbonding stabilization of the bound N_2.

2.2. Formation of End-on Bridging N_2 Species.

After the formation of a terminally coordinated N_2 ligand, the lone pair of the distal nitrogen can form a bond to a second transition metal center to give a $M_2(\mu\text{-}N_2)$ complex. This species is important because it undergoes N–N bond scission in the N_2 cleavage mechanism in Scheme 1 above. This section focuses on recent studies that have probed the pathways that lead to end-on bridging N_2 complexes, with a focus on systems that go on to form nitride complexes (as described in Section 4 below).

2.2.1. Electrochemically Induced Formation of N_2-Bridged Complexes. A comprehensive mechanistic study of reductive N_2 cleavage in the transformation of $(PNP^{tBu})ReCl_2$ to $(PNP^{tBu})Re(N)Cl$ provided key insight into the elementary steps associated with formation of a bridging N_2 intermediate, $[(PNP^{tBu})ReCl]_2(\mu\text{-}N_2)$ (PNP^{tBu} is $(({}^t Bu_2PCH_2CH_2)_2N)$.[117,118] The electrochemical and chemical steps leading to the N_2-bridged species occur at appropriate rates for CV analysis, as revealed by comparison of cyclic voltammograms collected under Ar and N_2 (Figure 8). Whereas a $1e^-$ reduction that exhibited increased reversibility with increasing scan rate or increasing Cl^- concentration was observed under Ar, an anodically shifted, irreversible $2e^-$ reduction was observed under N_2. The changes in peak potential and peak current as a function of scan rate and Cl^- concentration suggested an ECCE mechanism with "potential inversion", wherein the product of an intermediate chemical reaction is easier to reduce than the starting material.[118] The product of the $2e^-$ reduction under N_2 was identified as $[(PNP^{tBu})ReCl]_2(\mu\text{-}N_2)$ by spectroelectrochemical UV-Vis studies (Figure 8).

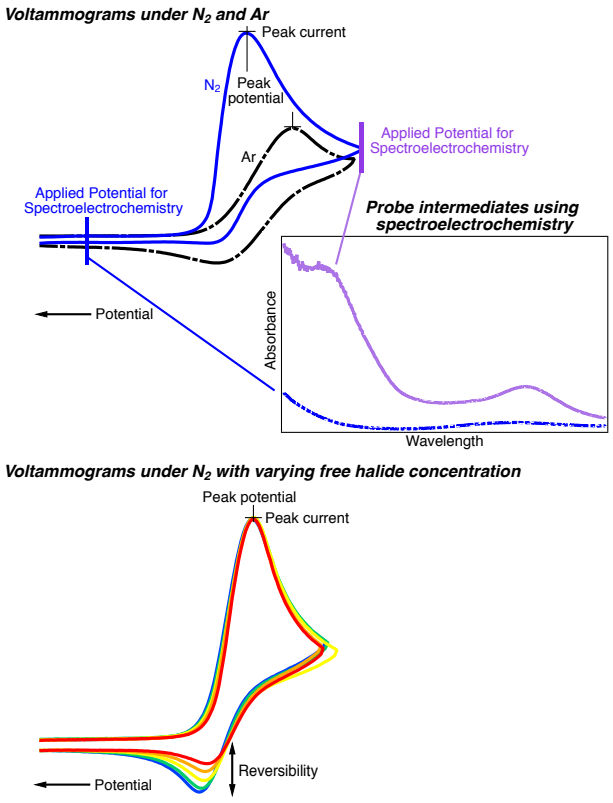

Figure 8. Electrochemical studies of $(PNP^{tBu})ReCl_2$.[118]

The mechanism of N_2 bridge formation was elucidated by varying the concentrations of $(PNP^{tBu})ReCl_2$, Cl^-, or N_2, with CV changes revealing a mechanism wherein reduction of $(PNP^{tBu})ReCl_2$ is followed by rapid N_2 association and subsequent Cl^- loss to give a Re^{II} N_2 complex, $(PNP^{tBu})ReCl(N_2)$, that is rapidly reduced to a Re^{I} intermediate (Scheme 2). The Re^{I} intermediate finally comproportionates with Re^{III} starting material as the species diffuse to/from the electrode surface (Scheme 2). Digital simulations of the voltammograms provided estimates of rate constants for each individual step. The use of "sensitivity tests," which examined how changing each rate constant affected the overall agreement, increased confidence in the simulations.[119,120]

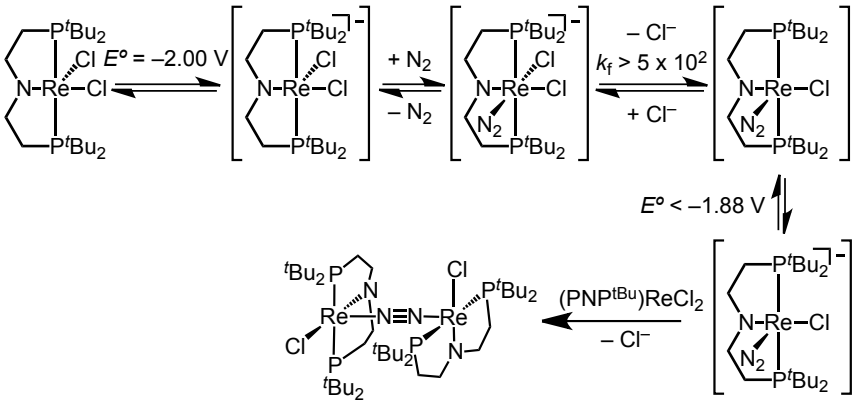

Scheme 2. Electrochemical mechanism of formation of $[(PNP^{tBu})ReCl]_2(\mu\text{-}N_2)$. Species in brackets were implicated but not isolated.[118]

A closely related Re dichloride complex featuring a monoanionic unsaturated ligand, $(^{dv}PNP^{tBu})ReCl_2$ (Figure 9), also binds N_2 upon electrochemical reduction, and the resulting ReNNRe species subsequently splits the N–N bond to yield two nitride complexes.[121] CV studies under Ar enabled a comparison of the reduction potential and rate constant for Cl^- dissociation. The potential for reduction to $[(^{dv}PNP^{tBu})ReCl_2]^-$ is 230 mV more anodic than that of $[(PNP^{tBu})ReCl_2]^-$, and the product releases Cl^- with a rate constant that is 10 times smaller.[118,121] Given the similar steric profiles of these ligands, this difference is attributed to the unsaturated backbone rendering the amide a weaker π-donor.[122] This suggests a similar tradeoff as noted above for terminal N_2 complexes: less electron-donating ligands enable reduction at milder potentials, but also generate a less electron-rich metal center that leads to slower Cl^- dissociation.

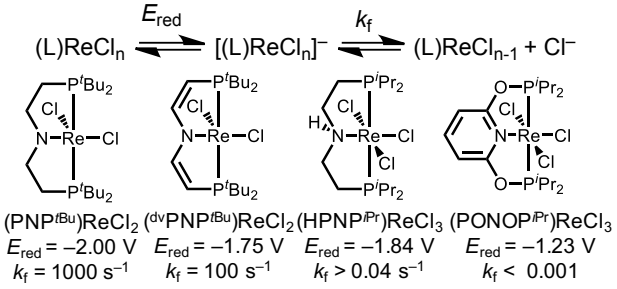

Figure 9. Summary of reduction potentials and chloride dissociation rate constants from rhenium pincer complexes.[118,121,123,124]

Two recent studies of Re complexes of neutral PNP pincer ligands provided further opportunities for structure-function comparisons. Schneider *et al.* examined the reductive chemistry of the diphosphinoamine complex $(HPNP^{iPr})ReCl_3$ (Figure 9).[123] Miller, Hasanayn, Holland, Mayer *et al.* studied the bis(phosphinito)pyridine complex $(PONOP^{iPr})ReCl_3$ (Figure 9).[124] These sterically similar complexes offer some interesting contrasts. The mechanisms of each system are summarized in Scheme 3.

The reduction potential of $(HPNP^{iPr})ReCl_3$ (–1.84 V) is 0.6 V more negative than that of $(PONOP^{iPr})ReCl_3$ (–1.23 V), Figure 9. The reduced species $[(HPNP^{iPr})ReCl_3]^-$ dissociates Cl^- and binds N_2. In contrast no electrochemically induced N_2 binding is observed upon reduction of $(PONOP^{iPr})ReCl_3$, and the isolable Re^{II} trichloride complex $[(PONOP^{iPr})ReCl_3]^-$ is obtained instead.[124] DFT studies using a THF continuum solvation model suggest that Cl^- dissociation from $[(PONOP^{iPr})ReCl_3]^-$ is endergonic by more than 20 kcal/mol,[124] which precludes electrochemically induced N_2 binding even though the net reaction to form the bridging N_2 complex $[(PONOP^{iPr})ReCl_2]_2(\mu\text{-}N_2)$ was predicted to be thermodynamically favorable (Scheme 3). The complex with the amine backbone, $(HPNP^{iPr})ReCl_3$, undergoes electrochemical reduction to give the N_2-bridged complex $[(HPNP^{iPr})ReCl_2)]_2(\mu\text{-}N_2)$ (Scheme 3). The steric profiles (based on percent buried volume, $\%V_{bur}$)[125] of the pincer ligands in $(HPNP^{iPr})ReCl_3$ ($\%V_{bur}$ = 58.9%) and $(PONOP^{iPr})ReCl_3$ ($\%V_{bur}$ = 57.7%) are similar, suggesting that the differences in Cl^- dissociation kinetics stem from electronic differences.[123,124] The less electron-rich metal center again makes Cl^- dissociation less favorable. The N_2 cleavage reactivity of these systems is discussed in Section 4.

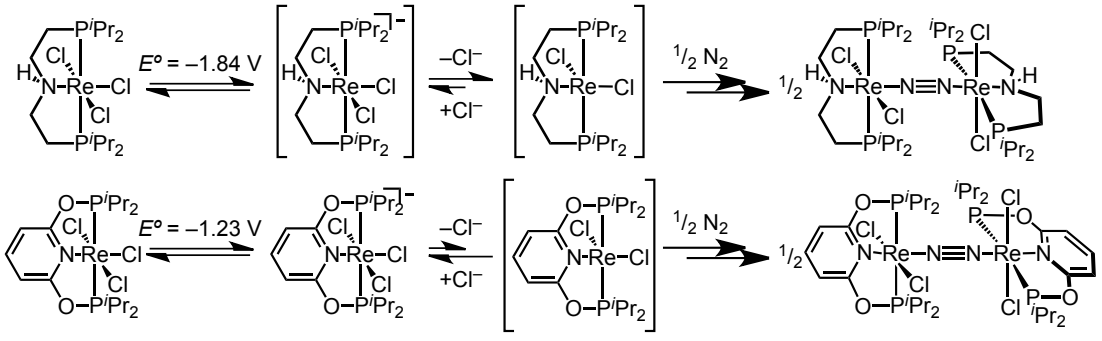

Scheme 3. Comparison of $(L_3)ReCl_3$ mechanisms. Species in brackets were implicated but not isolated.

2.2.2. Oxidative Electrochemical Formation of N_2-Bridged Complexes. A wealth of complexes are known that feature the $Mo_2(\mu\text{-}N_2)$ fragment.[99] Even though no electrochemical investigations of the reductive formation of a $Mo_2(\mu\text{-}N_2)$ species from N_2 have been described, a $Mo_2(\mu\text{-}N_2)$ core has been generated upon *oxidation* of the monomeric N_2 complex *trans*-$[(depe)_2Mo(N_2)_2]$, both electrochemically and using the chemical oxidant $[FeCp_2][BAr^F{}_4]$ (Ar^F = 3,5-bis(trifluoromethyl)phenyl), Scheme 4.[98] After oxidation, a nitride complex produced by N–N cleavage $[(depe)_2Mo(N)][BAr^F{}_4]$ was isolated.

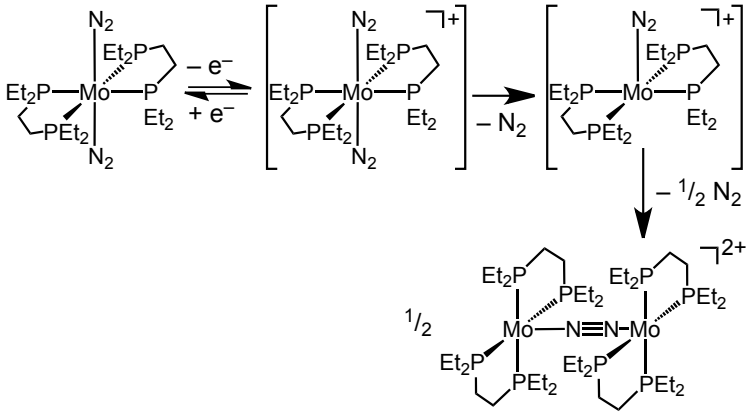

Scheme 4. Mechanism of electrochemical formation of $[\{(depe)_2Mo\}_2(\mu\text{-}N_2)]^{2+}$. Species in brackets are proposed but not isolated.[98]

The mechanism was examined using UV-Vis and resonance Raman (rR) spectroelectrochemistry (Scheme 4). UV-Vis-spectroelectrochemistry experiments in conjunction with time-dependent DFT provided support for a mechanism involving $1e^-$ oxidation to form *trans*-$[(depe)_2Mo(N_2)_2]^+$, followed by subsequent N_2 dissociation to yield $[(depe)_2Mo(N_2)]^+$ (k_{diss} = 0.0002 s^{-1}). Then, a dimerization step produced the direct precursor to N_2 cleavage, $[\{(depe)_2Mo\}_2(\mu\text{-}N_2)]^{2+}$, which was detected by rR-spectroelectrochemistry.[98] The oxidative process demonstrates the conversion of a terminal N_2 complex to a bridging N_2 complex (with concomitant dissociation of three N_2 ligands).

2.3. Insights into N_2 Electroreduction Catalyst Design

Electrochemical methods can probe the individual steps involved in reductive N_2 binding. In many cases, one or more steps occur on timescales that are amenable to kinetic analysis by variable scan rate CV studies. Slower steps can be analyzed using spectroelectrochemical methods

monitoring UV-vis, IR, or rR spectra of intermediates. This section highlights a few trends from mechanistic studies that could be relevant to the design of electrocatalysts for N_2 reduction.

In terms of thermodynamics, N_2 generally binds more strongly to more electron-rich metal centers. The kinetic factors that control N_2 binding are the same as any substitution reaction:[126,127] the coordination number, the electron-richness of the metal, the steric bulk around the metal center, and the identity of dissociating ligand(s). Low-coordinate complexes enable direct measurements of N_2 binding and can proceed in an associative fashion, whereas coordinatively saturated complexes often require (potentially rate-limiting) ligand dissociation before N_2 binding. One dissociating ligand that rarely has been studied is NH_3, which is surprising because reductive substitution of N_2 for NH_3 is a critical step of an electrocatalytic N_2 reduction cycle.[12,50,111,122] Schrock *et al.* examined the reduction potentials of Mo-NH_3 complexes, including measurement of the equilibrium constant for N_2/NH_3 substitution.[128] In another example that uses the aforementioned (TPB)Fe system, Peters *et al.* showed that an iron(II) amido complex (TPB)Fe(NH_2) could be protonated to afford $[(TPB)Fe(NH_3)]^+$, which upon reduction spontaneously dissociated NH_3 and bound N_2.[111] A key balance in the design of electrocatalysts, however, is the desire to operate at mild potentials while still effectively binding N_2: more negative reduction potentials tend to correlate with stronger N_2 binding, but typically result in higher overpotentials in a catalytic process.

The solvent is also a key parameter, intertwined with the substitution chemistry described above. The solvent must be capable of solvating a suitable supporting electrolyte. Different solvents will vary in the ability to solvate halides that often dissociate upon reduction during N_2 binding. If the solvent is also a good donor ligand, it can compete with N_2. In some cases, solvent can bind first, before slowly being displaced by N_2; in other cases, solvent binding may prevent N_2 binding altogether. Ethers such as THF and Et_2O often strike a balance between solvating ability and donor strength. In the future, other solvent candidates should be considered. For example, ionic liquids have been widely used in CO_2 electroreduction,[129] while alkyl carbonates that are commonly used in battery electrochemistry[130] have not yet been evaluated for N_2 reduction to our knowledge. A final consideration is the electrochemical window of the solvent. For example, arenes have a relatively narrow electrochemical reduction window while ethers or ionic liquids can offer access to a wider range of potentials.

3. Molecular Orbital Aspects of N_2 Binding

Although N_2 must bind initially as a terminal ligand to a single metal, the ultimate product may feature a terminal or a bridging N_2 binding mode, depending on the free energy of equation 1.

$$2\ M–N_2 \rightleftarrows N_2 + M–N{\equiv}N–M \qquad (1)$$

As judged by the NN stretching frequency (ν_{NN}), the N–N bond in complexes with an end-on bridging binding mode is typically weaker than in complexes with a terminal binding mode. The activation of N_2 by one or two metal centers is often understood in terms of the electronic structure of the π-systems of the terminal and bridging species,[131–134,67,135] which are described qualitatively in Figure 10.

In a terminal M–N_2 complex, the metal has a pair of *d* orbitals having π-symmetry with respect to the M–N bond. These AOs have the same symmetry as both the filled π– and empty π∗–MOs of N_2, though MO diagrams usually show only the interaction with π^*_{N2} due to the poor energy match and overlap between the *d* orbitals and π_{N2}. If it binds a second metal to form an end-on/end-on bridging MNNM species, there are two pairs of metal *d*-π AOs. These two pairs combine into pairs of e_u and e_g symmetry-adapted linear combinations (SALCs). The e_g SALC mixes with the π* orbital of the bridging N_2 to give a delocalized MO labeled $1\pi_g$. The e_u SALC, on the other hand, mixes with the filled π_{N2} (though the overlap is poor) to give $2\pi_u$.

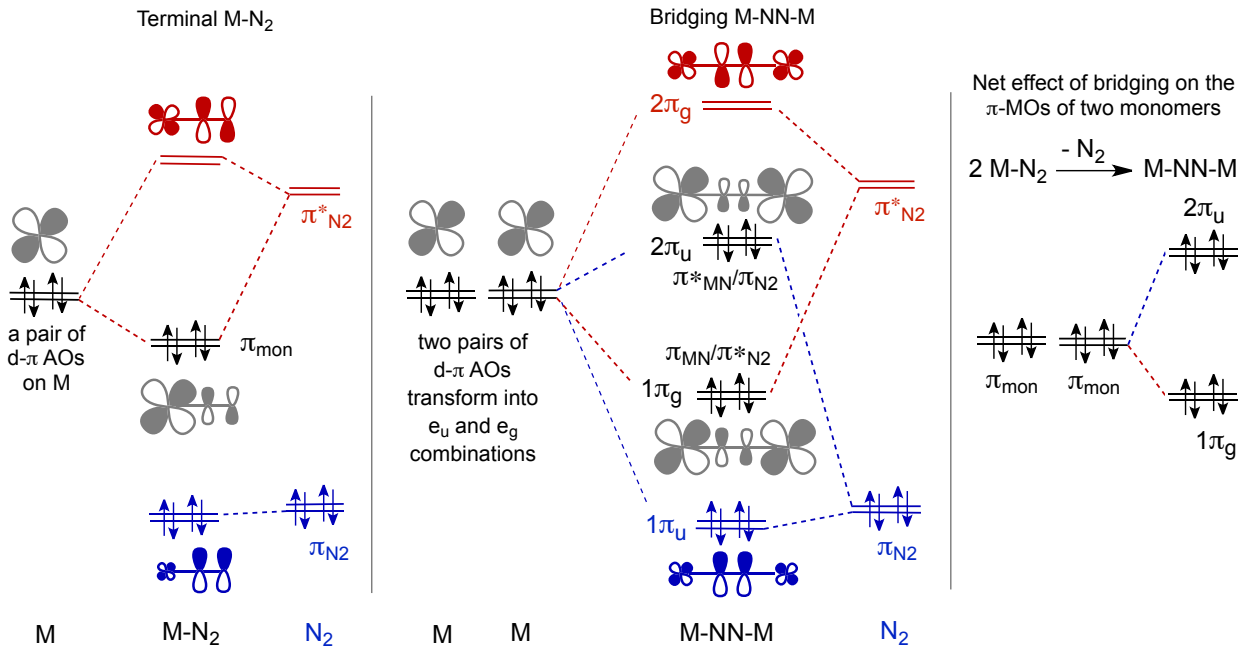

Figure 10. MO diagram illustrating key π-orbital interactions in terminal and bridging metal-N_2 bonds.

This model predicts correctly that the extent of NN weakening in a bridged complex, which is typically measured by way of the NN stretching frequency, depends on the population of the $1\pi_g$ and $2\pi_u$ MOs. The $1\pi_g$ MO is MN bonding and NN antibonding (π_{MN}/π^*_{NN}), so its increased population leads to increased weakening of the NN bond and a lower ν_{NN} value. The $2\pi_u$ MO is MN antibonding and NN bonding (π^*_{MN}/π_{NN}), so populating it actually strengthens the NN bond.[136] The detailed composition of the MOs depends on the geometry and identity of the metal, which can influence the energy and polarization of the metal orbitals. It is nevertheless instructive to examine some different π-orbital occupations. The $(1\pi_g)^2(2\pi_u)^0$ configuration is exemplified by a bridging discandium(II) complex (d^1-d^1), which shows moderate weakening with ν_{NN} = 1676 cm^{-1}.[137] Many d^2-d^2 systems give a $(1\pi_g)^4(2\pi_u)^0$ configuration, which weakens the NN bond much more, giving ν_{NN} values near 1300 cm^{-1} in dicationic Mo^{IV} and dianionic Nb^{III} complexes.[88,138] Partial filling of the $2\pi_u$ MO to give the $(1\pi_g)^4(2\pi_u)^2$ configuration retains a significant degree of NN activation; thus ν_{NN} in Mo^I, Mo^{III}, and Re^{II} μ-N_2 complexes is typically lower than 1800 cm^{-1},[124,139] and can be as low as 1290 cm^{-1}.[98,117] Even though it may seem counterintuitive for a system engaged in π-backbonding, incremental population of $2\pi_u$ in related complexes was

experimentally shown to systematically decrease the N–N distance or increase ν_{NN}.[93,138] Finally, the $(1\pi_g)^4(2\pi_u)^4$ configuration leads to minimal NN weakening, which is frequently observed in N_2 complexes of late transition metals. For example, $[\{Ru(NH_3)_5\}_2(\mu\text{-}N_2)]^{4+}$ has a relatively high NN stretching frequency of 2060 cm^{-1}.[140] Other examples of μ-N_2 complexes with $(1\pi_g)^4(2\pi_u)^4$ configurations include $[(^{tBu4}PCP)Ir]_2(\mu\text{-}N_2)$ and $[(^{tBu4}PNP)Mo(N_2)_2]_2(\mu\text{-}N_2)$ which have ν_{NN} = 1980 and 1890 cm^{-1}, respectively.[73,141]

Next, we extend this model to compare terminal to bridging end-on N_2 binding, by viewing the bridging species in a hypothetical equilibrium with two complexes having terminally bound N_2 (Figure 10, right). In this thought experiment, the energy levels of the four localized π_{mon} MOs split into two pairs of delocalized π–MOs, one pair of lower energy ($1\pi_g$) and one pair of higher energy ($2\pi_u$). This analysis predicts that there should be little π-stabilization upon dimerization when the π_{mon} MOs of the two terminal N_2-complexes are filled, because bridging would form a MNNM core with a $(1\pi_g)^4(2\pi_u)^4$ configuration that gains little from π-backbonding, and thus the terminal form would be favored. In agreement with this proposal, many late transition metal complexes have filled π_{mon} orbitals and exist as terminal N_2 complexes that show little tendency to bridge through N_2. The square planar d^8 complex $(^{tBu4}PCP)Ir(N_2)$, for example, binds N_2 in a terminal fashion at room temperature, with only very small amounts of the corresponding bridging complex under 1 atm N_2 at equilibrium. As an example from the middle of the transition series, the numerous d^6 complexes of the form M(diphosphine)$(N_2)_2$ (M = Mo, W), described in Section 2, also have filled π_{mon} orbitals and have terminal N_2 ligands.

When the π_{mon} orbitals of the two terminal N_2 complexes are not filled, Figure 10 predicts energetic stabilization upon attracting a second metal to form a bridging N_2 complex. This has been experimentally verified when electrons are removed from M(diphosphine)$(N_2)_2$ complexes: while Mo(dppe)$_2(N_2)_2$ (with filled π_{mon} orbitals) has terminal N_2 ligands, $1e^-$ oxidation results in formation of a bridging N_2 complex (with a $(1\pi_g)^4(2\pi_u)^2$ configuration of the MNNM core).[98] To our knowledge, all of the activated μ-N_2 complexes with $(1\pi_g)^4(2\pi_u)^2$ and $(1\pi_g)^4(2\pi_u)^0$ electron configurations mentioned above in the context of NN activation have no stable monometallic forms under N_2. In another instructive contrast, consider the $(1\pi_g)^4(2\pi_u)^2$ complex $[(PONOP^{iPr})ReCl_2]_2(\mu\text{-}N_2)$, which requires heating to 130 °C for one hour to incorporate $^{15}N_2$,

suggesting that access to the analogous monometallic Re^{II}–N_2 species (assumed to be intermediates in the exchange process) is highly endothermic. On the other hand, the complex $[(^{tBu4}PNP)Mo(N_2)_2]_2(\mu\text{-}N_2)$ incorporates $^{15}N_2$ in both the terminal and bridging positions at room temperature, because the N_2 bridge is more easily disrupted in this MNNM complex that has a $(1\pi_g)^4(2\pi_u)^4$ configuration. Note that the number of electrons in $1\pi_g$ and $2\pi_u$ is not necessarily the same as the total *d*-electron count, so some knowledge of the metal spin state and orbital occupancies within a given geometry is needed to be able to apply this model. Of course, the π-electronic effect does not completely govern the trend toward terminal vs. bridging N_2. Steric effects can prevent the formation of bimetallic complexes with bridging N_2. A notable series of examples come from Peters, which incorporate extremely bulky tripodal phosphine ligands that prevent bridging of N_2.[80,109,110,142]

4. N≡N Bond Cleavage: Structural and Electronic Considerations

The first example of direct N_2 cleavage by a transition metal complex, equation 2, was reported by Laplaza and Cummins in 1995.[82]

$$2\ L_nM + N_2 \rightarrow L_nM\text{–}NN\text{–}ML_n \rightarrow 2\ L_nM{\equiv}N \qquad (2)$$

Exposure of solutions of the molybdenum(III) complex $Mo[N(^tBu)(Ar)]_3$ (Ar = 3,5-dimethylphenyl) to an atmosphere of N_2 led to rapid and quantitative formation of the molybdenum(VI) terminal nitride complex $Mo(N)[N(^tBu)(Ar)]_3$. The reaction was proposed to proceed by initial binding of N_2 in a terminal fashion before generating an end-on N_2-bridged dimolybdenum complex that splits into two molybdenum(VI) nitride complexes.[139] This extraordinary reaction has remained rare in the following two decades, with only a few other complexes reported to be capable of bimetallic N_2 splitting.[94,143]

In this section, we discuss the structural and electronic factors that control the kinetics and thermodynamics of N_2 cleavage. These principles can help guide the development of molecular electrocatalysts where cleavage of the N≡N bond in an N_2-bridged intermediate is a key step.

4.1. Thermal N_2 Cleavage

Figure 11 gives a qualitative correlation diagram adapted from prior descriptions that follows the relevant MOs involved in the cleavage of representative $[L_nM]_2(\mu\text{-}N_2)$ complexes into two nitride complexes.[136,138,139,143,144] The analysis assumes idealized D_{3h} (n = 3) or D_{4h} (n = 4 or

5) symmetries. As in Figure 10, the diagram accounts for the π–MOs of the dimer resulting from the pairs of d_{xz}/d_{yz} orbitals on each metal center and the π and π* MOs of N_2, which transform into two pairs of e_u and e_g delocalized π–MOs. However, since the N–N bond can be broken completely, the diagram also considers the filled σ $(1a_g)^2$ and empty σ* $(1a_u)$ MOs from the MNNM skeleton.

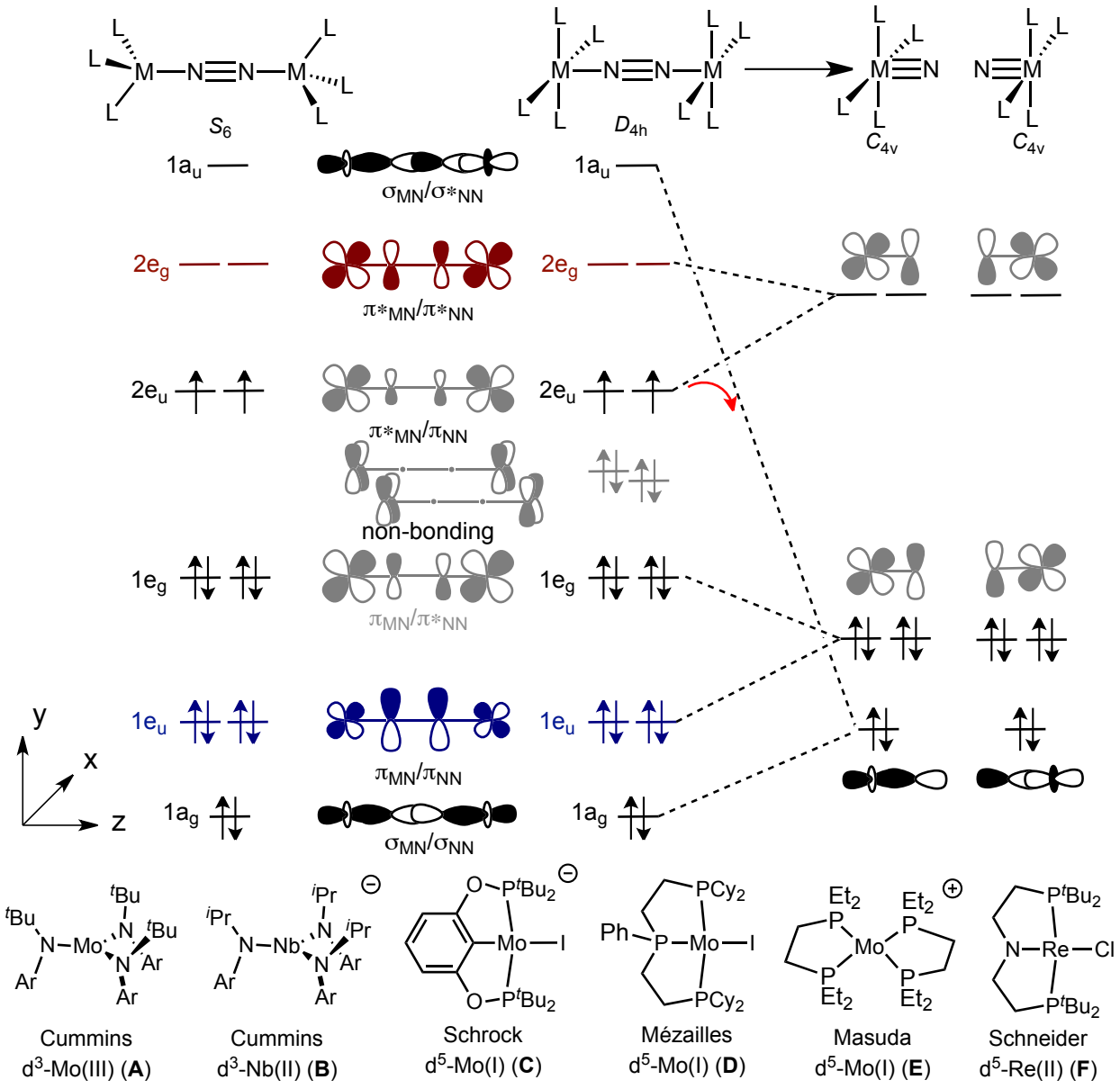

Figure 11. Qualitative MO diagram for $[(L_n)M]_2(\mu\text{-}N_2)$ complexes that cleave into metal-nitrides. Adapted from ref [139]. Ar = 3,5-$C_6H_3Me_2$. Molecular L_3M and L_4M fragments that are found in N_2 cleavage sequences are shown at bottom.

First, we consider N_2 cleavage by two d^3 metal centers with L_3M structures. For a $[(L_3)Mo]_2(\mu\text{-}N_2)$ system, as in the one derived from fragment **A**, each Mo^{III} center provides three electrons to the π-system, so the valence π-electron configuration is $(1e_u)^4(1e_g)^4(2e_u)^2(2e_g)^0$

(described below as "10-π"). SQUID magnetometry of the N_2-bridged complex provides experimental support for such a triplet ground state.[139] The filling of the $1e_g$ MO greatly diminishes the π-bond order of N_2 and increases the bond order of the two M-N bonds. In contrast, $2e_u$ is NN bonding and MN anti-bonding, so the partial filling of $2e_u$ does not contribute to NN cleavage nor to MN bond making. The empty high-energy $1a_u$ σ-MO is MN bonding and NN antibonding. Thus, if the two unpaired electrons of $2e_u$ are paired in $1a_u$ (red arrow in Figure 11), the NN bond order becomes zero.

Calculations by Morokuma *et al.* were the first to show that μ-N_2 cleavage in this system takes place on the closed shell singlet potential energy surface (PES) via a transition state (TS) having a zigzag geometry.[145] Simplistically, as the symmetry of the reactant is lowered along the reaction coordinate, the σ*-MO drops in energy dramatically, and becomes filled with the two unpaired electrons that were initially in the $2e_u$ π-MO, thus breaking one π-NN bond and making a new σ-MN bond. In the process, the remaining four delocalized $1e_u$ and $1e_g$ π-MOs with 8 electrons (four from the metals and four from N_2) that already had bonding MN character in the reactant μ-N_2 complex transform into four localized MN π-MOs with 8 electrons. These DFT calculations predicted the cleavage barrier via the zigzag transition state to be low. Experimentally, the kinetic barrier for cleavage of $[(ArRN)_3Mo]_2(\mu\text{-}N_2)$ (R = $C(CD_3)_2CH_3$, Ar = 3,5-$C_6H_3Me_2$) was determined to be $\Delta G^{\ddagger}$ = 22 kcal/mol at 298 K.[139]

The electron occupation in this system thus confers upon the product nitride maximal stability, with an MN bond order of three. As described in Section 4.3, the strong metal nitride bonding is critical for providing thermodynamic driving force to break the triple bond of N_2. Strikingly, however, initial DFT calculations by Morokuma *et al.* on a simplified model system predicted the net transformation from two Mo fragments (**A** in Figure 11) and one N_2 molecule to two MoN nitrides to be exothermic by more than 100 kcal/mol. Additional calculations by Neyman supported this conclusion and suggested that unusually strong relativistic effects play a role in formation of strong MoN bonds in this system.[146] Subsequently, Hoff and Nolan measured the MoN bond dissociation enthalpy (BDE) value, which can be combined with the BDE of N_2 to estimate ΔH = –86 kcal/mol in toluene.[147]

The importance of a 10-π configuration in d^3/d^3 systems is also apparent in studies of heterobimetallic Mo/Nb complexes.[148] The N_2-bridged complex $(L_3)Mo(\mu\text{-}N_2)Nb(L'_3)$, derived

from fragments **A** and **B** in Figure 11, does not cleave N_2, which can be attributed to the d^3/d^2 system providing only a 9-π configuration. One-electron reduction in this system prompts formation of the respective Mo and Nb nitrides, presumably via a 10-π intermediate.

Turning to systems $[(L_4)M]_2(\mu\text{-}N_2)$ with N_2 bridging two d^5 metal centers, the π-bonding picture is much the same as in $[(L_3)Mo]_2(\mu\text{-}N_2)$ with two d^3 metal centers. The additional electrons in the d^5/d^5 D_{4h} complexes occupy two δ-symmetry MOs from the in-phase and out-of-phase combinations of the metal d_{xy} orbitals, which are orthogonal to the MNNM axis and labelled as non-bonding in the MO diagram. Note that the δ-MOs are empty in the S_6 symmetry complex and are engaged in π-bonding with the amido ligands, and thus they are omitted from the corresponding MO diagram. Thus, $\mu\text{-}N_2$ complexes derived from d^5 fragments, including complexes **C**,[92] **D**,[149] **E**,[98] and **F**[117] in Figure 11 above, have the same π-electron configuration as complex **A**, and all of these species undergo thermal N_2 cleavage to form stable nitride complexes. For the $\mu\text{-}N_2$ dimer derived from **F**, DFT calculations and spectroscopic experiments suggested a triplet ground state for the N_2 complex, which cleaves via a zigzag TS on the singlet PES (experimental and computational $\Delta G^{\ddagger}$ ca. 20 kcal/mol at 298 K).[118] The N_2 cleavage reaction was computed to be highly exergonic (–40 kcal/mol).

Figure 11 helps rationalize why some structurally related N_2-bridged complexes have not been observed to undergo N_2 cleavage.[143] For example, Cummins and coworkers demonstrated that removal of one or two electrons from $[(L_3)Mo]_2(\mu\text{-}N_2)$ suppresses N_2 cleavage altogether.[138] The monocationic and dicationic dimers have 9 and 8 π-electrons, respectively, so the nitride complexes resulting from N_2 cleavage would be expected to have reduced bond orders and therefore less driving force for N–N cleavage.

A 10-π configuration in a $\mu\text{-}N_2$ complex is *not sufficient* to drive cleavage, however. For example, the $\mu\text{-}N_2$ dimers derived from the molybdenum(III) and rhenium(II) fragments **G**,[150] **H**,[117,118] and **I**[124] in Figure 12 all have 10-π configurations, yet they are all isolable and stable to cleavage of the $\mu\text{-}N_2$ group. For example, DFT calculations predict insurmountable kinetic barriers ($\Delta G^{\ddagger}_{298}$ is 42 kcal/mol for **H** and 51-53 kcal/mol for **I**) and endergonic thermodynamics (ΔG°_{298} is 2 kcal/mol for **H** and 10-14 kcal/mol for **I**) for cleavage in these Re systems.

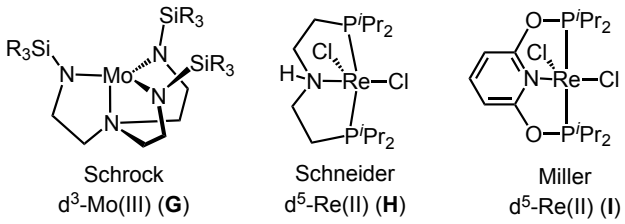

Figure 12. Mo (SiR_3 = Si^tBu_2Me) and Re complexes that form bimetallic complexes with ligands *trans* to the N_2 bridge.

This different behavior can be attributed to the presence of a ligand *trans* to each of the μ-N_2 atoms in the given class of complexes.[124] A bridging N_2 ligand has a much weaker *trans* influence than the nitride ligand, as shown by structural comparison of the μ-N_2 dimer of **I** and its octahedral nitrido monomer.[124] Specifically, the Re–Cl bond *trans* to μ-N_2 in the *cis,trans* isomer of the dimer from **I** elongates from 2.41 Å to 2.64 Å when it becomes *trans* to the nitride ligand upon cleavage. The weakening of the two bonds *trans* to μ-N_2 can render the N_2 cleavage reaction unfavorable. The zigzag TS exhibits a large degree of metal-nitride character, so the free energy of activation increases when ligands are coordinated *trans* to the μ-N_2 ligand. Computational studies predicted that sequential removal of chloride ligands from N_2-bridged complexes derived from **I** would render the N_2 cleavage reaction increasingly thermodynamically favorable and kinetically accessible.[124] These results suggest that an empty coordination site *trans* to the bridging N_2 ligand is conducive to kinetically facile and thermodynamically favorable μ-N_2 cleavage in systems with 10 π-electron configurations.

While the present analysis has focused on electronic structure, N_2 cleavage reactivity is also strongly influenced by the steric bulk of the supporting ligands. Appropriate steric protection is important for preventing formation of M–M bonds and for labilizing ligands such as halides.[151] Large supporting ligands can also provide access to low-coordinate N_2 dimers with a vacant site *trans* to the N_2 bridge. After N_2 cleavage, bulky supporting ligands can prevent formation of bridging nitride products,[99] which are typically less reactive due to the engagement of the terminal lone pair.

4.2. Photochemical N_2 Cleavage.

A few examples of four-coordinate $[(L_3)Mo]_2(\mu\text{-}N_2)$[91,138] and six-coordinate $[(L_5)M]_2(\mu\text{-}N_2)$ (M = Mo[93], Re[123,124]) complexes are capable of N_2 cleavage to form terminal nitride complexes

only upon UV irradiation (Figure 13). All of these examples of photochemical N_2 cleavage have a 10-π configuration.[91,93,123,124,138] A study by Nishibayashi *et al.* suggests that the 10-π configuration is important: in the redox series $[\{(depf)Mo(Cp^*)\}_2(\mu\text{-}N_2)]^{n+}$ (Figure 13, $n = 0$, 1, or 2; depf is 1,1'-bis(diethylphosphino)ferrocene), only the neutral complex, which has a 10-π electronic configuration, undergoes photochemical N_2 cleavage. The oxidized complexes, $n = 1$ (9-π configuration) and $n = 2$ (8-π configuration), do not photochemically generate nitride complexes despite more strongly activated N–N bonds.[93] Several dinuclear complexes cleave under illumination despite having a ligand *trans* to the bridging N_2, even though as noted above this geometry disfavors thermal N_2 cleavage. Efforts to further investigate the mechanisms of photochemical N_2 cleavage have been predominantly computational,[93,123,138] and a general orbital explanation for photochemical N_2 cleavage has not yet emerged. Even the nature of unproductive pathways remains obscure, although one can imagine the possibility of pathways such as photochemical cleavage of M–N_2 bonds;[152] some recent time-resolved studies have begun to examine vibrational coupling and relaxation pathways.[153–155]

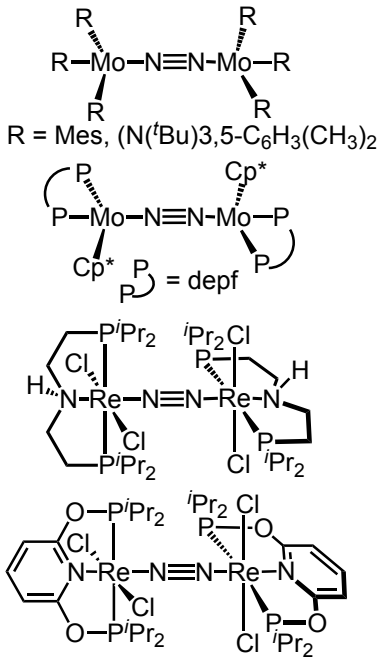

Figure 13. Examples of $M_2(\mu\text{-}N_2)$ species that undergo N_2 cleavage upon irradiation.

In some cases, photochemical N_2 cleavage of $[(L_5)M]_2(\mu\text{-}N_2)$ to form nitride complexes $(L_5)MN$ is thermodynamically disfavored (endergonic).[123,124] These systems are exciting examples

of photon energy being stored in the form of nitride complexes. However, though thermal N–N coupling back to N_2 should be thermodynamically feasible, these nitrides complexes typically encounter high kinetic barriers to thermal reversion. For example, formation of nitride complex $(PONOP^{iPr})Re(N)Cl_2$ is computed to be uphill by 10 kcal/mol, yet the photochemical nitride product does not dimerize back to a bridging N_2 complex and can be subsequently converted to NH_4^+.[124]

Photochemical N_2 cleavage can also connect electrochemically generated bridging $M_2(\mu\text{-}N_2)$ with subsequent N_2-fixation reactions via terminal nitride intermediates. In a recent example, $[(HPNP^{iPr})ReCl_2]_2(\mu\text{-}N_2)$ was generated via bulk electrolysis before *in situ* photolysis generated $(HPNP^{iPr})Re(N)Cl_2$.[123] This photoelectrochemical N_2 cleavage reaction allowed subsequent synthesis of N_2-derived benzonitrile to complete a synthetic cycle for N_2 fixation.

4.3 Thermochemistry and the Periodic Trends Relevant to N_2 Cleavage.

The N≡N triple bond in N_2 is one of the strongest chemical bonds, with a bond dissociation enthalpy of 226 kcal/mol.[156] An analysis of N_2 splitting should therefore consider the thermodynamic challenges associated with cleavage of this strong bond. Considering the strong bond of N_2, thermodynamically favorable formation of two metal nitrides from N_2 (eq 2 above) requires that the products have very strong MN bonds, likely >113 kcal/mol. The Mo–N bond dissociation enthalpy of the Mo^{VI} nitride $Mo(N)(NRAr)_3$ (based on the fragment **A** in Figure 11 above) was experimentally determined to be ΔH^o = 155 kcal/mol.[147] Overall N_2 splitting reactions are also entropically unfavorable, as three molecules are converted to two.

To break such strong M≡N triple bonds in terminal nitride complexes requires that both σ and π bonding be strong. In addition to the orbital considerations described above, the electropositive nature and propensity for formation of strong π-bonds can help explain the N_2 cleavage reactivity of metals along the diagonal from vanadium to rhenium on the left half of the periodic table. For later metals, such as osmium, the thermochemistry of N_2 cleavage is such that it proceeds in the opposite direction, forming N_2 from two species $L_nOs{\equiv}N$.[157,158] For earlier metals, strong M–N σ bonds are formed but the π bonds are weaker, and in these cases N_2 cleavage often proceeds to form bridging nitride complexes.[99]

4.4. Design Principles for N_2 Cleavage.

The structural and electronic trends that have emerged provide guidance for the design of new systems capable of facile N_2 cleavage (Figure 14). A strong metal–nitride bond is paramount. In addition to electronegativity and orbital overlap considerations, a 10-π configuration in the N_2-bridged dimer that precedes N_2 cleavage helps provide the thermodynamic driving force for nitride formation. N–N bond cleavage can be kinetically facile, even though it requires a spin state change and distortion of the linear M–N–N–M unit to a zig-zag configuration, provided there is a vacant site *trans* to the bridging N_2 ligand in the reactant (and therefore *trans* to the nitride in the product). Bulky ligands can use steric effects to help access low-coordinate intermediates to facilitate low-barrier, exergonic N_2 cleavage. MNNM complexes with a 10-π configuration and a *trans* ligand tend to undergo N_2 cleavage reactions that are less thermodynamically favorable and more kinetically demanding, but these can sometimes be driven by photolysis (so far with high-energy photons). An overarching challenge facing catalyst development is that the most kinetically facile N_2 cleavage reactions are so exergonic as to produce very stable nitride complexes that exact a steep energetic price for further reactivity at the nitride. Strategies are needed to achieve relatively isoergic N_2 cleavage, as seen for complexes with ligands *trans* to the N_2 bridge, but with low kinetic barriers for nitride formation.

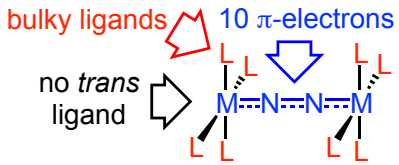

Figure 14. Overview of some factors that promote favorable kinetics and thermodynamics of N_2 cleavage.

5. Characterizing and Tuning the Reactivity of N_2-Derived Nitride Complexes

5.1 Overview of Nitride Reactivity.

Terminal nitride ligands are commonly characterized as either "nucleophilic" or "electrophilic,"[159–163] and several factors can influence their observed reactivity trends. The relative energy of metal *d*-orbitals and nitride *p*-orbitals, for example, affects the localization of antibonding molecular orbitals in a metal nitride complex (Figure 15).[164] The MN-π* orbitals gain more N character as the energy of metal *d*-orbitals is lowered, such that late transition metal complexes produce better orbital overlap with incoming nucleophiles (electrophilic reactivity);

conversely, the MN σ- and π-symmetry orbitals gain more N character as the energy of metal *d*-orbitals is raised, such that earlier transition metal nitride complexes are more nucleophilic.

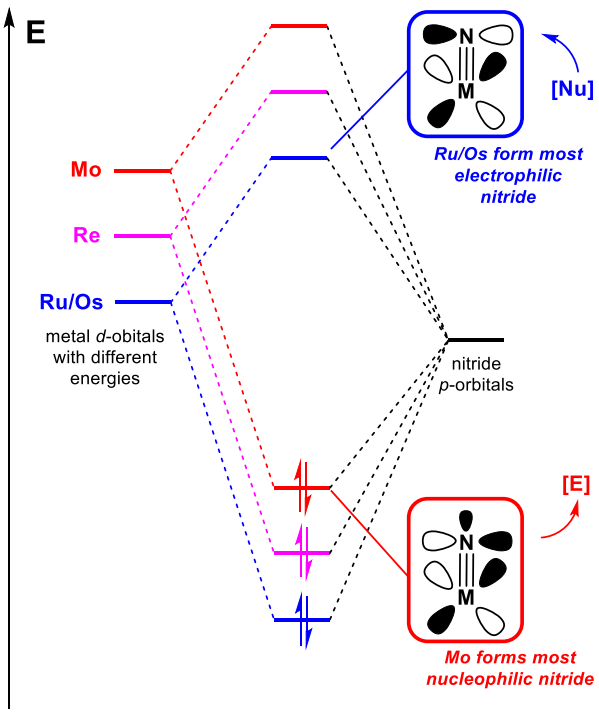

Figure 15. Qualitative MO diagram for metal nitrides with different *d*-orbital energies.

The N_2-derived Mo nitride discovered in his group has been described by Cummins as a "reluctant nucleophile".[165] This description has proven to be quite appropriate for many nitride complexes derived from N_2, which often require forcing reaction conditions for functionalization. The difficulty in coaxing N_2-derived nitride complexes into productive reactions can be traced to the thermodynamic stability described in Section 4.3. Approaches to destabilize metal-nitride interactions include changing the oxidation state of the metal in order to increase nucleophilicity or encourage radical character on the nitride,[166–168] modifying or replacing the supporting ligands,[123,168,169] installing a ligand *trans* to the nitride,[123] and utilizing exogenous Lewis acids or electrophiles to activate the nitride.[165]

5.2. Case study in tuning nitride complex reactivity.

Schneider's N_2-derived pincer-supported Re nitrides provide an excellent example of how modifying the supporting ligand can facilitate organic synthesis starting from N_2. The N_2-derived Re^{V}-nitride complexes $(PNP^{tBu})Re(N)(Cl)$[169] and $(HPNP^{iPr})Re(N)(Cl)_2$[123] each react with carbon

electrophiles *en route* to organic nitriles. The five-coordinate complex (PNP^{tBu})Re(N)(Cl) requires benzyl triflate for N–C bond formation, while the six-coordinate complex (HPNP^{iPr})Re(N)(Cl)$_2$ reacts with benzoyl chloride. This reactivity can be attributed to enhanced nucleophilicity of the nitride when it lies *trans* to a Cl$^-$ ligand. The weaker metal-nitride interaction is reflected in a Re–N distance that is 0.03 Å longer in the six-coordinate vs. five-coordinate complex.

Mayer and Holland recently reported additional studies on the oxidative chemistry of (PNP^{tBu})Re(N)(Cl) with ligand modifications that can be done *in situ*. Chemical oxidation of the PNP ligand to form a nitroxide followed by 1e^- outer sphere oxidation results in [(P^{O}NP)Re(N)(Cl)]$^+$, which displays electrophilic reactivity with phosphines (Figure 16).[168] Phosphinimide formation from [(P^{O}NP)Re(N)(Cl)]$^+$ occurs more rapidly with electron-rich phosphines, indicating an *umpolung* from the nucleophilic nitride in (PNP^{tBu})Re(N)(Cl) to an electrophilic nitride in [(P^{O}NP)Re(N)(Cl)]$^+$. Spectroscopic and computational data indicate that the Re-nitride interaction weakens upon oxidation, and the LUMO becomes more localized at the nitride ligand. This identifies a potential strategy of directly modifying the coordinated supporting ligand of metal nitrides in order to influence reactivity at the nitride ligand.

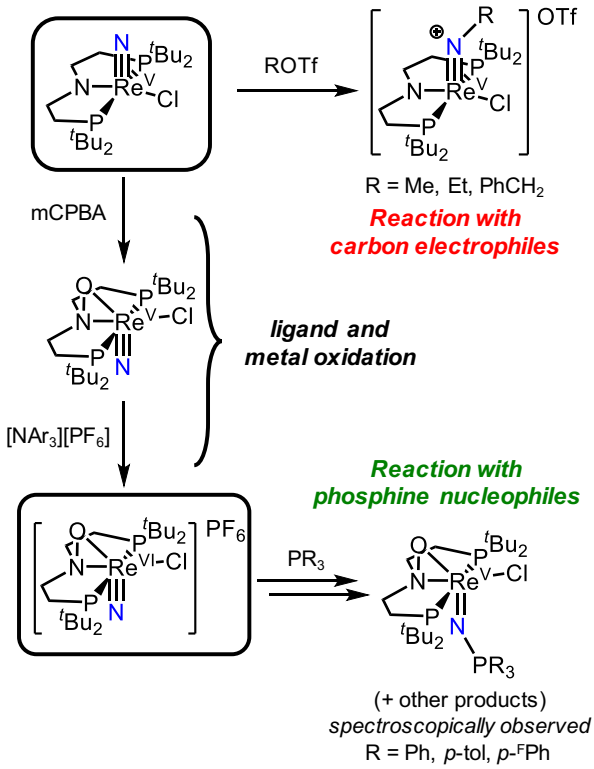

Figure 16. Reversal of Re-nitride behavior from nucleophilic to electrophilic following chemical oxidation of the supporting ligand and oxidation of the metal center.

5.3 Trends in Enabling Reactivity at N_2-Derived Nitride Ligands

Existing synthetic routes utilizing N_2 typically require strong reductants to generate the nitrides and strong electrophiles for nitride functionalization, which can cause problems when the reagents for these steps are incompatible. To achieve catalysis, the energetics of N_2 cleavage and nitride functionalization must be balanced. One possible approach relies on reversible *in situ* ligand modifications to modulate nitride reactivity. For example, the aliphatic backbones in PNP-pincer ligands can reversibly donate H^+/e^- equivalents to promote nitride reduction.[123,170] Rationally incorporating H^+/e^- reservoirs into the supporting ligand may be a powerful tool during catalysis, where reductive conditions can regenerate the ligand as well as split N_2. An alternative ligand modification could involve a ligand that toggles between an electron-rich form that enables facile N_2 cleavage and an electron-poor form that leads to a more reactive nitride product. These strategies would leverage the properties of the supporting ligand to generate a reactive metal-nitride without hindering prerequisite N_2 cleavage at the metal center.

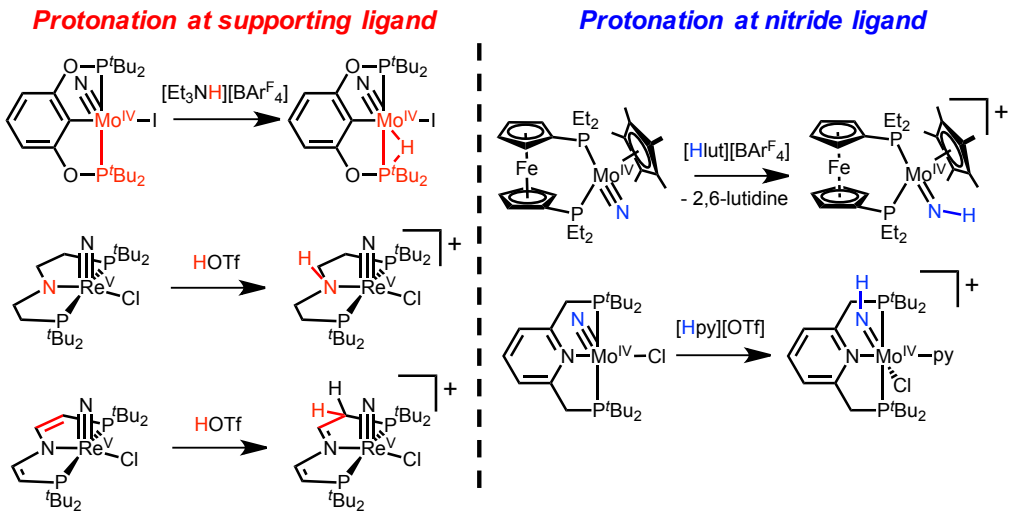

Figure 17. Left: Unproductive protonation at the supporting ligands of N_2-derived nitride complexes. **Right:** Productive protonation of N_2-derived nitrides to form imide complexes.

While N_2-derived nitrides show promise as "reluctant nucleophiles" in reactions with organic electrophiles, these nitrides rarely react productively with proton sources. Protonation of N_2-derived metal nitrides often occurs at the supporting ligand or metal center rather than the nitride ligand (Figure 17, left).[123,139,165,168] Considering the many examples of Mo in molecular catalysts for ammonia synthesis, it is unsurprising that productive protonation of group 6 nitride complexes has been reported (Figure 17, right),[94,124] sometimes accompanied by coordination of

the conjugate base or counterion. The rarity of direct nitride protonation highlights the need for approaches to N_2 electroreduction to NH_3 that do not rely on nitride protonation. An approach to imide formation from N_2-derived metal nitrides has been to utilize a proton-coupled electron transfer strategy, which we examine in the following section.

6. Nitride conversion to ammonia using PCET

6.1. Matching N–H Bond Strengths with PCET Reagents.

The electrosynthesis of NH_3 via an N_2 cleavage step can be broken into two halves: the N_2 cleavage process to form a metal nitride complex and the subsequent nitride conversion to NH_3. The latter process requires a $3H^+/3e^–$ reduction of the N_2-derived nitride complex, making it a proton-coupled electron transfer (PCET) challenge. Considering that the thermodynamic potential of N_2 reduction to NH_3 is close to 0 V, the thermodynamics of the two halves of a catalytic N_2-to-NH_3 cycle must offset each other, because the overall process is approximately ergoneutral. When the typical N_2 cleavage processes that form the metal nitrides are highly exergonic, the PCET nitride reductions to NH_3 must therefore be highly endergonic. Strong reductants and Brønsted acids are thus required to achieve the N–H bond formations needed to make NH_3.

A thermochemical "square scheme" for the first PCET to a metal-nitride is presented in Figure 18. PCET can occur via stepwise proton transfer (PT) followed by electron transfer (ET), by stepwise ET followed by PT, or by concerted ET and PT. Initial PT is controlled by the nitride basicity (imido pK_a, blue in Figure 18), while the initial ET is controlled by the reduction potential of the nitride complex ($E°$, red in Figure 18). A concerted PCET mechanism (Figure 18, purple) couples H^+ and $e^–$ transfer into one elementary step. The thermodynamic favorability of PCET depends on the relative bond dissociation free energy (BDFE) values of the N–H bond being formed and the $H^+/e^–$-donating PCET reagent(s). Even when the H^+ and $e^–$ come from separate reagents, an "effective BDFE" ($BDFE_{eff}$) can be assigned to the acid/reductant pair.[171,172]

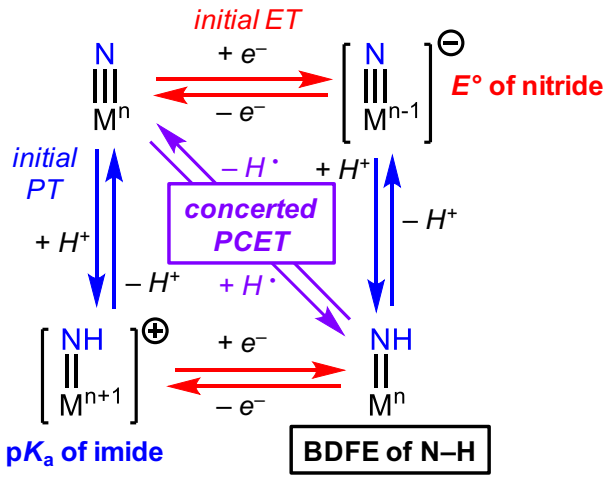

Figure 18. Thermochemical square scheme for the PCET reduction of an N_2-derived nitride ligand to an imide showing stepwise (red/blue) and concerted (purple) pathways.

The N–H BDFE of the imide complex can be used to predict reactivity with various PCET reagents; however, experimental data for these M=NH complexes is lacking.[173] Computational studies have suggested that, for several systems, the first N–H bond is weaker and that the strength of subsequent N–H bonds increases with formation of the amide and ammine ligand (Figure 19).[124,174–176] Figure 19 compares theoretically estimated N–H BDFE values of N_2-derived imide/amide/amine complexes with BDFE (or $BDFE_{eff}$) values of a range of PCET reagents. Many commonly utilized PCET reagents contain X–H bonds (BDFE ~ 60–80 kcal/mol) that are likely too strong to render imide N–H bond formation (highlighted in red in Figure 19) exergonic. Reagents that are generated *in situ* upon the pairing of a reductant and acid are more promising, with $BDFE_{eff}$ ~ 25–60 kcal/mol.

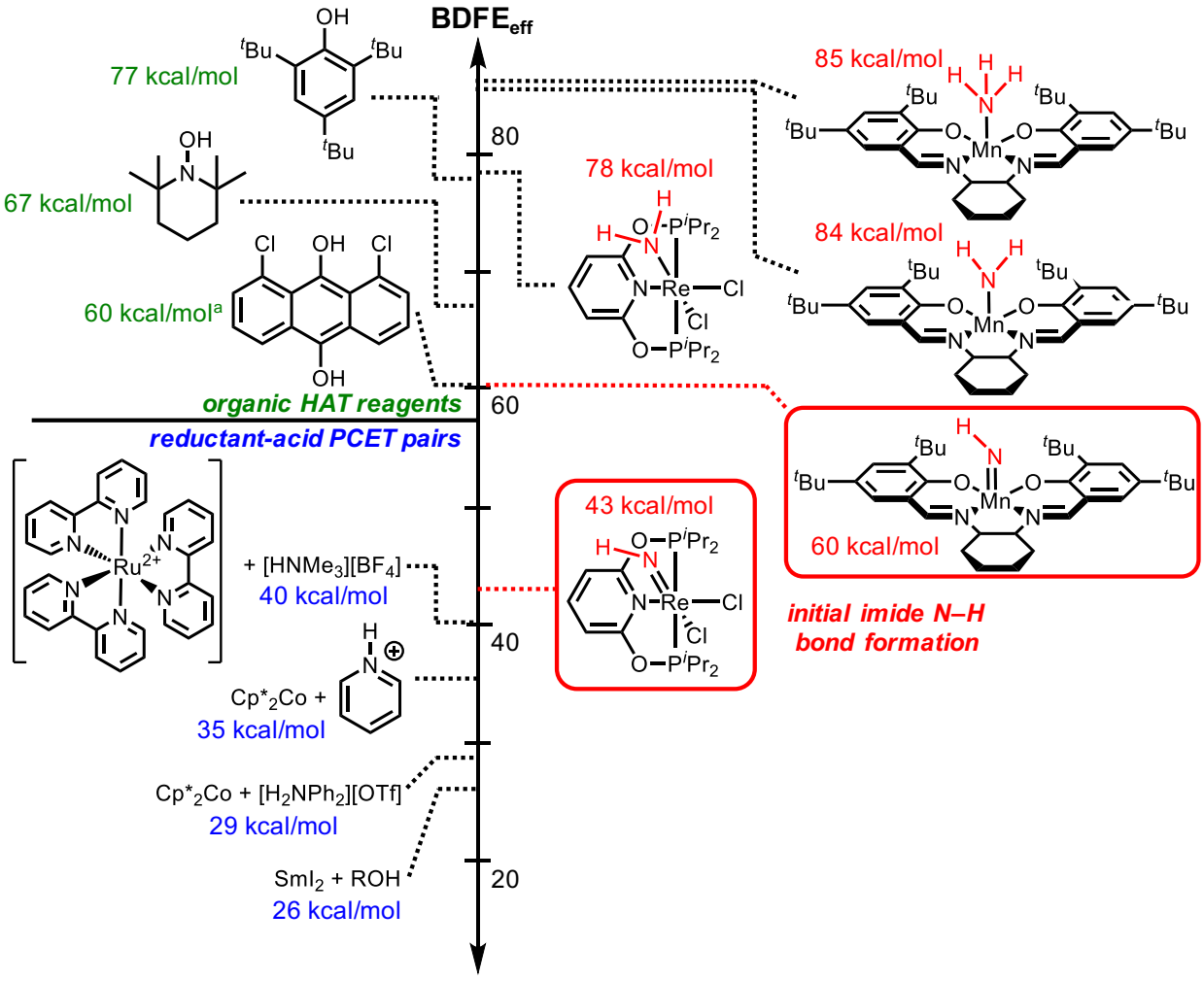

Figure 19. Comparison of effective bond-dissociation free energy ($BDFE_{eff}$) values for various PCET reagents and imide, amide, and ammine N–H bonds. **Left:** Experimental values for unimolecular reagents (green) and reductant-acid pairs (blue). [a]Average O–H BDFE in H_2O.[177] **Right:** DFT calculated N–H BDFEs in THF.[124,175]

Two classes of PCET reagents have been the focus of important recent studies in N_2 reduction, with both acid/metallocene and samarium/water pairings providing multicomponent systems with exceptionally weak effective BDFE values.

6.2. PCET involving Acid/Metallocene Combinations.

The combination of metallocene reductants and anilinium acids has been particularly successful in NH_3 synthesis (Figure 20). Recent studies have revealed the formation of [(Cp*)(*exo*-η^4-C_5Me_5H)Co]$^+$ by protonation of Cp*$_2$Co at low temperatures, which implies that concerted

PCET could happen directly from this single species.[50,178,179] The PCET pathway enabled by metallocenes results in a four-fold higher yield of NH_3 by Cp_2*Co/$[H_2NPh_2][OTf]$ as compared to KC_8/$[H][BAr^F{}_4]$ in N_2 reduction catalyzed by the Fe complex of Figure 20A, even though the KC_8-based method provides higher driving force. The yields of these reactions are greater at low temperatures, which mirrors the stability of the PCET reagent $[(Cp^*)(exo\text{-}\eta^4\text{-}C_5Me_5H)Co]^+$, which persists at low temperatures.[179] In catalytic reactions employing pyridinium acids, a similar concerted PCET mechanism has been proposed involving the pyridinyl radical ($BDFE_{eff}$ ~ 35 kcal/mol), although it lacks as much experimental support.[174,180]

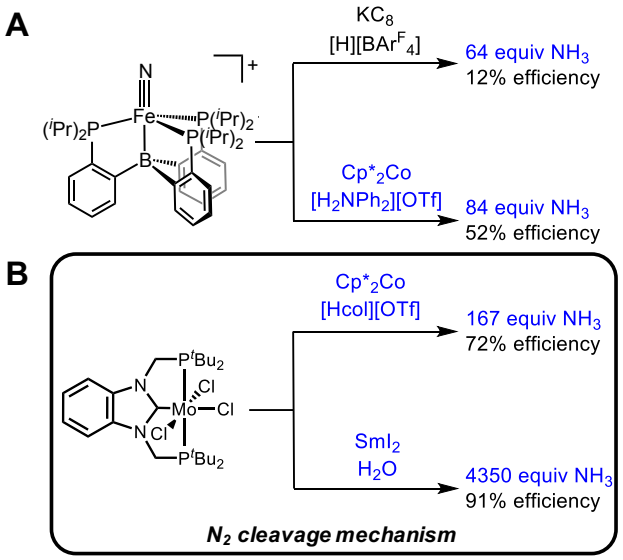

Figure 20. Catalytic N_2 to NH_3 systems that proceed through a nitride intermediate. Reactions with reductant-acid PCET pairs that can generate strong HAT reagents are shown in blue. The efficiency is defined as yield NH_3 based on amount of reductant added. col = collidinium.

(TPB)Fe represents the only molecular system for electrocatalytic N_2 reduction to NH_3 reported so far. Under N_2 at –35 °C, the electrolysis of (TPB)Fe (–2.1 V) can generate up to 5.5 equiv NH_3 per Fe in the presence of 50 equiv of $[H_2NPh_2][OTf]$ and at least 1 equiv of $Cp^*{}_2Co$, operating with a Faradaic efficiency of ~20% (Figure 21).[50] Electrochemical turnover is enhanced by addition of at least 1 equiv of $Cp^*{}_2Co$, implicating $[(Cp^*)(exo\text{-}\eta^4\text{-}C_5Me_5H)Co]^+$ as a PCET mediator. It is likely that this involves PCET to a nitride, since chemical catalysis of N_2 reduction to NH_3 proceeds through a nitride intermediate $[(TPB)Fe(N)]^+$, although this nitride is not thought to derive from bimetallic N_2 cleavage.

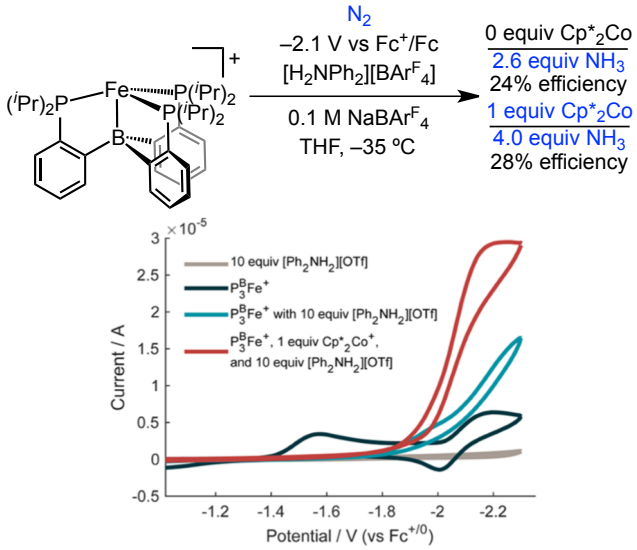

Figure 21. N_2 electroreduction to NH_3 catalyzed by a molecular (TPB)Fe system. The system shows an enhancement in NH_3 yield and Faradaic efficiency upon addition of Cp^*_2Co as a HAT mediator (**top**), which corresponds to an enhancement in cathodic current passed during cyclic voltammetry experiments (**bottom**, red trace). Reproduced with permission from ref. [50] (Copyright, 2018, American Chemical Society).

6.3. PCET Involving SmI_2/H_2O.

The combination of SmI_2 and H_2O (or alcohols), which has been extensively studied for organic transformations,[181–183] is noteworthy for having the weakest $BDFE_{eff}$ reported to date (26 kcal/mol).[183] Remarkably, SmI_2/H_2O displays very slow rates of H_2 evolution, despite substantial thermodynamic driving force.[184]

Nishibayashi and coworkers recently demonstrated that the combination of SmI_2 and H_2O can be used as the reductant-acid pair for catalytic N_2 reduction to NH_3 using Mo-pincer complexes (Figure 20B). Utilizing this system, which is proposed to proceed through N_2 cleavage to form a Mo^{IV}-nitride intermediate,[100] they report much higher turnover numbers for N_2 reduction to NH_3 than other known systems, with up to 90% selectivity for NH_3 over H_2.[97]

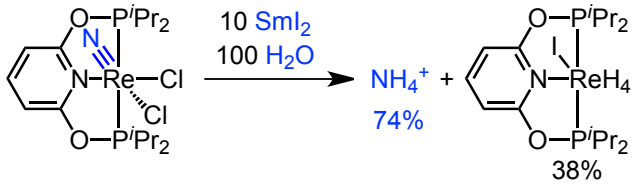

Scheme 5. PCET reduction of $(PONOP^{iPr})Re(N)(Cl)_2$ to release ammonia.

SmI_2/H_2O was recently employed for the PCET reduction of the N_2-derived rhenium(V) nitride complex $(PONOP^{iPr})Re(N)(Cl)_2$, resulting in fixation of N_2 to NH_3 (Scheme 5). This system

is particularly notable considering the extremely weak N–H bond formed from initial nitride reduction to the imide (N–H BDFE = 42 kcal/mol).[124] The use of SmI_2/H_2O renders formation of the first N–H bond exergonic by ca. 20 kcal/mol, and formation of the second N–H bond exergonic by as much as 60 kcal/mol (Figure 19). While the imide N–H bond is thermodynamically favored to release H_2,[173,176,185] the strong driving force for amide formation may enable rapid PCET from SmI_2/H_2O that favors NH_3 production (although some H_2 is indeed generated during the reaction).

6.4. Outlook on PCET Ammonia Formation.

Because imide and amide complexes often have weak N–H BDFE values, it is crucial to discover new acid/reductant combinations that have weak (effective) BDFE values and are kinetically stable with respect to H_2 evolution. One promising approach utilizes photoexcitation to overcome the challenge of "bottling" reagents with weak BDFEs. The photoreductant-acid pair $[Ru(bpy)_3]^{2+}/HNMe_3^+$, for example, successfully reduced a nitride (not N_2-derived) to NH_3 and could be regenerated by the sacrificial reductant dihydroacridine.[175,186]

Overall, the factors that determine N–H bond strengths along the pathway from nitride to NH_3 are not yet well understood. This is in part due to the small number of systems capable of producing NH_3 from N_2-derived nitride complexes, which limits the ability to collect and compare thermochemical data to identify trends. Insight into N–H bond formation at metal nitrides will be important in the design of future systems.

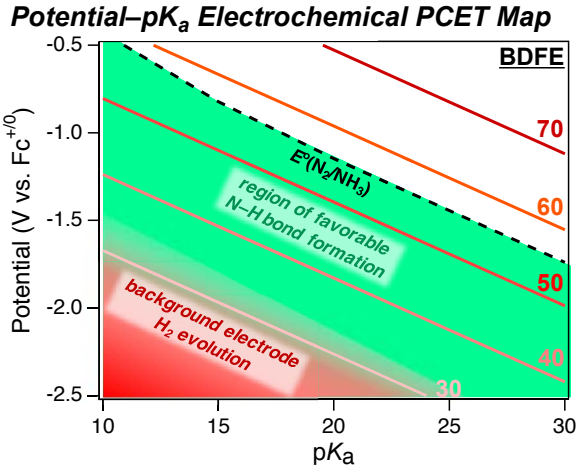

Figure 22. Potential–pK_a map in MeCN (bottom) of favorable N–H bond forming regions.

The success of acid/reductant pairs augurs further development of electrochemical systems, where the potential at the electrode and pK_a of the acid employed can be independently tuned to

control the effective BDFE for PCET.[12,50] Figure 22 shows how different combinations of reductants and acids can achieve the same effective BDFE values. With knowledge of the N–H BDFE of interest, or the MN_xH_y reduction potential, appropriate acids or acid/reductant pairs can be chosen for the desired reaction. PCET at electrode surfaces often follows different mechanisms than molecular reactions in solution, with pre-organization of substrates prior to PCET, such as through hydrogen bonding, playing an important role.[187,188] Alternatively, the PCET steps in an electrocatalytic N_2 reduction cycle could be achieved through the use of a molecular PCET mediator, as recently demonstrated by Peters and coworkers.[189,190]

7. Outlook on Ammonia Electrosynthesis via N_2 Cleavage.

Despite recent progress in electrochemical N_2 reduction to NH_3, there is still no report of a molecular electrocatalyst that operates by the N_2 cleavage pathway. However, each of the individual steps has been demonstrated, confirming the promise of this approach. Further support for this notion comes from the observation that leading Mo catalysts for NH_3 synthesis using chemical reductants appear to proceed via an N_2 cleavage mechanism.[97] Though these are currently driven by chemical reductants, we anticipate that some of these eventually will be adapted for electrocatalysis.

Looking ahead, some key challenges in electrocatalyst development can be identified. One prime consideration involves leveling the free energy surface between N_2 splitting and nitride PCET. The known examples of thermal N_2 cleavage are strongly exergonic, producing nitride intermediates that are thermodynamically resistant to N–H bond formation. An ideal system will mediate a nearly ergoneutral N_2 cleavage reaction to form a nitride that forms relatively strong N–H bonds. New insight into how ligands *trans* to N_2-derived ligands influence N_2 cleavage and nitride PCET may inspire new strategies relevant to this goal. Of practical concern is the accurate quantification of the NH_3 product and confirmation of its provenance from N_2.[191–196]

The N–H bond formation steps may involve mediators that can deliver H^+/e^- equivalents, or electroreduction with proton donors pre-organized via hydrogen bonding or other means. Because N_2 reduction to NH_3 and H^+ reduction to H_2 occur at similar potentials, ideal electrocatalysts must have kinetic selectivity for N_2 reduction pathways. The kinds of mechanistic insight that have been described here provide guidance in the design of new metal–ligand

combinations and selection of reaction conditions to optimize individual steps, and continued mechanism-guided development holds promise for electrocatalyst discovery.

Acknowledgements

This work was supported through the NSF Chemical Catalysis program under Grant Nos. CHE-1665135, CHE-1665137, and CHE-1665146. Q.J.B. acknowledges support from the NSF Graduate Research Fellowship Program (DGE-1650116). F.H. acknowledges support from LNCSR-AUB. We thank James Mayer for his contributions to our collaborative efforts, and for comments on this manuscript. We thank Sven Schneider, Inke Siewert, and their groups for establishing enjoyable and engaging collaborations that have strengthened many of the studies described here.

Supporting Information Statement

No supporting information.

References

(1) Erisman, J. W.; Sutton, M. A.; Galloway, J.; Klimont, Z.; Winiwarter, W. How a Century of Ammonia Synthesis Changed the World. *Nat. Geosci.* **2008**, *1*, 636–639.

(2) Smil, V. Enriching the Earth: Fritz Haber, Carl Bosch, and the Transformation of World Food Production; MIT Press: Cambridge, MA, 2004.

(3) Smil, V. Detonator of the Population Explosion. *Nature* **1999**, *400*, 415.

(4) Fritz Haber – Nobel Lecture. NobelPrize.org https://www.nobelprize.org/prizes/chemistry/1918/haber/lecture/ (accessed May 14, 2020).

(5) Carl Bosch – Nobel Lecture. NobelPrize.org. Nobel Media AB 2019 https://www.nobelprize.org/prizes/chemistry/1931/bosch/facts/ (accessed May 14, 2020).

(6) Ertl, G. Reactions at Surfaces: From Atoms to Complexity (Nobel Lecture). *Angew. Chem. Int. Ed.* **2008**, *47*, 3524–3535.

(7) Jennings, J. R. Catalytic Ammonia Synthesis; Jennings, J. R., Ed.; Fundamental and Applied Catalysis; Springer US: Boston, MA, 1991.

(8) Jewess, M.; Crabtree, R. H. Electrocatalytic Nitrogen Fixation for Distributed Fertilizer Production? *ACS Sustain. Chem. Eng.* **2016**, *4*, 5855–5858.

(9) Schlögl, R. Catalytic Synthesis of Ammonia—A "Never-Ending Story"? *Angew. Chem. Int. Ed.* **2003**, *42*, 2004–2008.

(10) Renner, J. N.; Greenlee, L. F.; Ayres, K. E.; Herring, A. M. Electrochemical Synthesis of Ammonia: A Low Pressure, Low Temperature Approach. *Interface Mag.* **2015**, *24*, 51–57.

(11) Bard, A. J.; Parsons, R.; Jordan, J. Standard Potentials in Aqueous Solution; M. Dekker: New York, 1985.

(12) Lindley, B. M.; Appel, A. M.; Krogh-Jespersen, K.; Mayer, J. M.; Miller, A. J. M. Evaluating the Thermodynamics of Electrocatalytic N_2 Reduction in Acetonitrile. *ACS Energy Lett.* **2016**, *1*, 698–704.

(13) Rosca, V.; Duca, M.; DeGroot, M. T.; Koper, M. T. M. Nitrogen Cycle Electrocatalysis. *Chem. Rev.* **2009**, *109*, 2209–2244.

(14) Amar, I.; Lan, R.; Petit, C. G.; Tao, S. Solid-State Electrochemical Synthesis of Ammonia: A Review. *J. Solid State Electrochem.* **2011**, *15*, 1845–1860.

(15) Giddey, S.; Badwal, S. P. S.; Munnings, C.; Dolan, M. Ammonia as a Renewable Energy Transportation Media. *ACS Sustain. Chem. Eng.* **2017**, *5*, 10231–10239.

(16) Kyriakou, V.; Garagounis, I.; Vasileiou, E.; Vourros, A.; Stoukides, M. Progress in the Electrochemical Synthesis of Ammonia. *Catal. Today* **2017**, *286*, 2–13.

(17) Liu, H.; Wei, L.; Liu, F.; Pei, Z.; Shi, J.; Wang, Z.; He, D.; Chen, Y. Homogeneous, Heterogeneous, and Biological Catalysts for Electrochemical N_2 Reduction toward NH_3 under Ambient Conditions. *ACS Catal.* **2019**, *9*, 5245–5267.

(18) Hochman, G.; Goldman, A. S.; Felder, F. A.; Mayer, J. M.; Miller, A. J. M.; Holland, P. L.; Goldman, L. A.; Manocha, P.; Song, Z.; Aleti, S. Potential Economic Feasibility of Direct Electrochemical Nitrogen Reduction as a Route to Ammonia. *ACS Sustain. Chem. Eng.* **2020**, *8*, 8938–8948.

(19) U.S. Energy Information Administration Annual Energy Outlook 2020; 2020.

(20) Ammonia: Catalysis and Manufacture; Nielsen, A., Ed.; Springer Berlin Heidelberg: Berlin, Heidelberg, 1995.

(21) Pindyck, R. S. The Social Cost of Carbon Revisited. *J. Environ. Econ. Manage.* **2019**, *94*, 140–160.

(22) Ricke, K.; Drouet, L.; Caldeira, K.; Tavoni, M. Country-Level Social Cost of Carbon. *Nat. Clim. Chang.* **2018**, *8*, 895–900.

(23) van der Ham, C. J. M.; Koper, M. T. M.; Hetterscheid, D. G. H. Challenges in Reduction of Dinitrogen by Proton and Electron Transfer. *Chem. Soc. Rev.* **2014**, *43*, 5183.

(24) Holland, P. L. Nitrogen Fixation. In *Comprehensive Inorganic Chemistry II*; McCleverty, J., Meyer, T. J., Eds.; Elsevier: Oxford, 2004; pp 569–599.

(25) Seefeldt, L. C.; Hoffman, B. M.; Peters, J. W.; Raugei, S.; Beratan, D. N.; Antony, E.; Dean, D. R. Energy Transduction in Nitrogenase. *Acc. Chem. Res.* **2018**, *51*, 2179–2186.

(26) Qing, G.; Ghazfar, R.; Jackowski, S. T.; Habibzadeh, F.; Ashtiani, M. M.; Chen, C.-P.; Smith, M. R.; Hamann, T. W. Recent Advances and Challenges of Electrocatalytic N_2 Reduction to Ammonia. *Chem. Rev.* **2020**, *120*, 5437–5516.

(27) Yang, D.; Chen, T.; Wang, Z. Electrochemical Reduction of Aqueous Nitrogen (N_2) at a Low Overpotential on (110)-Oriented Mo Nanofilm. *J. Mater. Chem. A* **2017**, *5*, 18967–18971.

(28) Zhang, L.; Ji, X.; Ren, X.; Ma, Y.; Shi, X.; Tian, Z.; Asiri, A. M.; Chen, L.; Tang, B.; Sun, X. Electrochemical Ammonia Synthesis via Nitrogen Reduction Reaction on a MoS_2 Catalyst: Theoretical and Experimental Studies. *Adv. Mater.* **2018**, *30*, 1800191.

(29) Chen, S.; Perathoner, S.; Ampelli, C.; Mebrahtu, C.; Su, D.; Centi, G. Electrocatalytic Synthesis of Ammonia at Room Temperature and Atmospheric Pressure from Water and Nitrogen on a Carbon-Nanotube-Based Electrocatalyst. *Angew. Chem. Int. Ed.* **2017**, *56*, 2699–2703.

(30) Liu, Y.; Su, Y.; Quan, X.; Fan, X.; Chen, S.; Yu, H.; Zhao, H.; Zhang, Y.; Zhao, J. Facile Ammonia Synthesis from Electrocatalytic N_2 Reduction under Ambient Conditions on N-Doped Porous Carbon. *ACS Catal.* **2018**, *8*, 1186–1191.

(31) Lee, H. K.; Koh, C. S. L.; Lee, Y. H.; Liu, C.; Phang, I. Y.; Han, X.; Tsung, C.-K.; Ling, X. Y. Favoring the Unfavored: Selective Electrochemical Nitrogen Fixation Using a Reticular Chemistry Approach. *Sci. Adv.* **2018**, *4*, eaar3208.

(32) Kugler, K.; Luhn, M.; Schramm, J. A.; Rahimi, K.; Wessling, M. Galvanic Deposition of Rh and Ru on Randomly Structured Ti Felts for the Electrochemical NH_3 Synthesis. *Phys.*

Chem. Chem. Phys. **2015**, *17*, 3768–3782.

(33) Kordali, V.; Kyriacou, G.; Lambrou, C. Electrochemical Synthesis of Ammonia at Atmospheric Pressure and Low Temperature in a Solid Polymer Electrolyte Cell. *Chem. Commun.* **2000**, 1673–1674.

(34) Wang, J.; Yu, L.; Hu, L.; Chen, G.; Xin, H.; Feng, X. Ambient Ammonia Synthesis via Palladium-Catalyzed Electrohydrogenation of Dinitrogen at Low Overpotential. *Nat. Commun.* **2018**, *9*, 1795.

(35) Song, Y.; Johnson, D.; Peng, R.; Hensley, D. K.; Bonnesen, P. V; Liang, L.; Huang, J.; Yang, F.; Zhang, F.; Qiao, R.; Baddorf, A. P.; Tschaplinski, T. J.; Engle, N. L.; Hatzell, M. C.; Wu, Z.; Cullen, D. A.; Meyer, H. M.; Sumpter, B. G.; Rondinone, A. J. A Physical Catalyst for the Electrolysis of Nitrogen to Ammonia. *Sci. Adv.* **2018**, *4*, e1700336.

(36) Qiu, W.; Xie, X.-Y.; Qiu, J.; Fang, W.-H.; Liang, R.; Ren, X.; Ji, X.; Cui, G.; Asiri, A. M.; Cui, G.; Tang, B.; Sun, X. High-Performance Artificial Nitrogen Fixation at Ambient Conditions Using a Metal-Free Electrocatalyst. *Nat. Commun.* **2018**, *9*, 3485.

(37) Han, J.; Ji, X.; Ren, X.; Cui, G.; Li, L.; Xie, F.; Wang, H.; Li, B.; Sun, X. MoO_3 Nanosheets for Efficient Electrocatalytic N_2 Fixation to NH_3. *J. Mater. Chem. A* **2018**, *6*, 12974–12977.

(38) Ren, X.; Cui, G.; Chen, L.; Xie, F.; Wei, Q.; Tian, Z.; Sun, X. Electrochemical N_2 Fixation to NH_3 under Ambient Conditions: Mo_2N Nanorod as a Highly Efficient and Selective Catalyst. *Chem. Commun.* **2018**, *54*, 8474–8477.

(39) Li, X.; Li, T.; Ma, Y.; Wei, Q.; Qiu, W.; Guo, H.; Shi, X.; Zhang, P.; Asiri, A. M.; Chen, L.; Tang, B.; Sun, X. Boosted Electrocatalytic N_2 Reduction to NH_3 by Defect-Rich MoS_2 Nanoflower. *Adv. Energy Mater.* **2018**, *8*, 1801357.

(40) Lv, C.; Yan, C.; Chen, G.; Ding, Y.; Sun, J.; Zhou, Y.; Yu, G. An Amorphous Noble-Metal-Free Electrocatalyst That Enables Nitrogen Fixation under Ambient Conditions. *Angew. Chem. Int. Ed.* **2018**, 6073–6076.

(41) Shi, M.-M.; Bao, D.; Wulan, B.-R.; Li, Y.-H.; Zhang, Y.-F.; Yan, J.-M.; Jiang, Q. Au Sub-Nanoclusters on TiO_2 toward Highly Efficient and Selective Electrocatalyst for N_2 Conversion to NH_3 at Ambient Conditions. *Adv. Mater.* **2017**, *29*, 1606550.

(42) Li, S.-J.; Bao, D.; Shi, M.-M.; Wulan, B.-R.; Yan, J.-M.; Jiang, Q. Amorphizing of Au Nanoparticles by CeO_X–RGO Hybrid Support towards Highly Efficient Electrocatalyst for N_2 Reduction under Ambient Conditions. *Adv. Mater.* **2017**, *29*, 1700001.

(43) Bao, D.; Zhang, Q.; Meng, F.-L.; Zhong, H.-X.; Shi, M.-M.; Zhang, Y.; Yan, J.-M.; Jiang, Q.; Zhang, X.-B. Electrochemical Reduction of N_2 under Ambient Conditions for Artificial N_2 Fixation and Renewable Energy Storage Using N_2/NH_3 Cycle. *Adv. Mater.* **2017**, *29*, 1604799.

(44) Kong, J.; Lim, A.; Yoon, C.; Jang, J. H.; Ham, H. C.; Han, J.; Nam, S.; Kim, D.; Sung, Y.-E.; Choi, J.; Park, H. S. Electrochemical Synthesis of NH_3 at Low Temperature and Atmospheric Pressure Using a γ-Fe_2O_3 Catalyst. *ACS Sustain. Chem. Eng.* **2017**, *5*,

10986–10995.

(45) Ren, X.; Zhao, J.; Wei, Q.; Ma, Y.; Guo, H.; Liu, Q.; Wang, Y.; Cui, G.; Asiri, A. M.; Li, B.; Tang, B.; Sun, X. High-Performance N_2-to-NH_3 Conversion Electrocatalyzed by Mo_2C Nanorod. *ACS Cent. Sci.* **2019**, *5*, 116–121.

(46) Pickett, C. J.; Talarmin, J. Electrosynthesis of Ammonia. *Nature* **1985**, *317*, 652–653.

(47) Denisov, N. T.; Shilov, A. E.; Shuvalova, N. I.; Panova, T. P. Mechanism of Electron Transfer in Dinitrogen Fixation in the System Ti(III)−Mo(III). *React. Kinet. Catal. Lett.* **1975**, *3*, 229–229.

(48) Becker, J. Y.; Avraham (Tsarfaty), S.; Posin, B. Nitrogen Fixation: Part I. Electrochemical Reduction of Titanium Compounds in the Presence of Catechol and N2 in MeOH or THF. *J. Electroanal. Chem. Interfacial Electrochem.* **1987**, *230*, 143–153.

(49) Efimov, O. N.; Strelets, V. V. Metal Complex Catalysis of Electrochemical Reactions. *Coord. Chem. Rev.* **1990**, *99*, 15–53.

(50) Chalkley, M. J.; Del Castillo, T. J.; Matson, B. D.; Peters, J. C. Fe-Mediated Nitrogen Fixation with a Metallocene Mediator: Exploring PK_a Effects and Demonstrating Electrocatalysis. *J. Am. Chem. Soc.* **2018**, *140*, 6122–6129.

(51) Chalkley, M. J.; Drover, M. W.; Peters, J. C. Catalytic N_2-to-NH_3 (or -N_2H_4) Conversion by Well-Defined Molecular Coordination Complexes. *Chem. Rev.* **2020**, *120*, 5582–5636.

(52) Mackay, B. A.; Fryzuk, M. D. Dinitrogen Coordination Chemistry: On the Biomimetic Borderlands. *Chem. Rev.* **2004**, *104*, 385–401.

(53) Gambarotta, S.; Scott, J. Multimetallic Cooperative Activation of N_2. *Angew. Chem. Int. Ed.* **2004**, *43*, 5298–5308.

(54) MacLeod, K. C.; Holland, P. L. Recent Developments in the Homogeneous Reduction of Dinitrogen by Molybdenum and Iron. *Nat. Chem.* **2013**, *5*, 559–565.

(55) Khoenkhoen, N.; de Bruin, B.; Reek, J. N. H.; Dzik, W. I. Reactivity of Dinitrogen Bound to Mid- and Late-Transition-Metal Centers. *Eur. J. Inorg. Chem.* **2015**, *2015*, 567–598.

(56) Légaré, M.-A.; Bélanger-Chabot, G.; Dewhurst, R. D.; Welz, E.; Krummenacher, I.; Engels, B.; Braunschweig, H. Nitrogen Fixation and Reduction at Boron. *Science* **2018**, *359*, 896.

(57) Légaré, M.-A.; Rang, M.; Bélanger-Chabot, G.; Schweizer, J. I.; Krummenacher, I.; Bertermann, R.; Arrowsmith, M.; Holthausen, M. C.; Braunschweig, H. The Reductive Coupling of Dinitrogen. *Science* **2019**, *363*, 1329.

(58) Sherbow, T. J.; Thompson, E. J.; Arnold, A.; Sayler, R. I.; Britt, R. D.; Berben, L. A. Electrochemical Reduction of N_2 to NH_3 at Low Potential by a Molecular Aluminum Complex. *Chem. – A Eur. J.* **2019**, *25*, 454–458.

(59) Evans, W. J.; Zucchi, G.; Ziller, J. W. Dinitrogen Reduction by Tm(II), Dy(II), and Nd(II) with Simple Amide and Aryloxide Ligands. *J. Am. Chem. Soc.* **2003**, *125*, 10–11.

(60) Lu, E.; Atkinson, B. E.; Wooles, A. J.; Boronski, J. T.; Doyle, L. R.; Tuna, F.; Cryer, J. D.; Cobb, P. J.; Vitorica-Yrezabal, I. J.; Whitehead, G. F. S.; Kaltsoyannis, N.; Liddle, S. T. Back-Bonding between an Electron-Poor, High-Oxidation-State Metal and Poor π-Acceptor Ligand in a Uranium(v)–Dinitrogen Complex. *Nat. Chem.* **2019**, *11*, 806–811.

(61) Mansell, S. M.; Kaltsoyannis, N.; Arnold, P. L. Small Molecule Activation by Uranium Tris(Aryloxides): Experimental and Computational Studies of Binding of N_2, Coupling of CO, and Deoxygenation Insertion of CO_2 under Ambient Conditions. *J. Am. Chem. Soc.* **2011**, *133*, 9036–9051.

(62) Falcone, M.; Chatelain, L.; Scopelliti, R.; Živković, I.; Mazzanti, M. Nitrogen Reduction and Functionalization by a Multimetallic Uranium Nitride Complex. *Nature* **2017**, *547*, 332.

(63) Falcone, M.; Barluzzi, L.; Andrez, J.; Fadaei Tirani, F.; Zivkovic, I.; Fabrizio, A.; Corminboeuf, C.; Severin, K.; Mazzanti, M. The Role of Bridging Ligands in Dinitrogen Reduction and Functionalization by Uranium Multimetallic Complexes. *Nat. Chem.* **2019**, *11*, 154–160.

(64) Hoffman, B. M.; Lukoyanov, D.; Yang, Z.-Y.; Dean, D. R.; Seefeldt, L. C. Mechanism of Nitrogen Fixation by Nitrogenase: The Next Stage. *Chem. Rev.* **2014**, *114*, 4041–4062.

(65) Sickerman, N. S.; Ribbe, M.; Hu, Y. 7. The Interstitial Carbide of the Nitrogenase M-Cluster: Insertion Pathway and Possible Function. In *Characterization, Properties and Applications*; Rouault, T., Ed.; De Gruyter: Berlin, Boston, 2017.

(66) Bjornsson, R.; Lima, F. A.; Spatzal, T.; Weyhermüller, T.; Glatzel, P.; Bill, E.; Einsle, O.; Neese, F.; DeBeer, S. Identification of a Spin-Coupled Mo(III) in the Nitrogenase Iron–Molybdenum Cofactor. *Chem. Sci.* **2014**, *5*, 3096–3103.

(67) McWilliams, S. F.; Holland, P. L. Dinitrogen Binding and Cleavage by Multinuclear Iron Complexes. *Acc. Chem. Res.* **2015**, *48*, 2059–2065.

(68) Hill, P. J.; Doyle, L. R.; Crawford, A. D.; Myers, W. K.; Ashley, A. E. Selective Catalytic Reduction of N_2 to N_2H_4 by a Simple Fe Complex. *J. Am. Chem. Soc.* **2016**, *138*, 13521–13524.

(69) Chatt, J.; Pearman, A. J.; Richards, R. L. The Reduction of Mono-Coordinated Molecular Nitrogen to Ammonia in a Protic Environment. *Nature* **1975**, *253*, 39–40.

(70) Chatt, J.; Dilworth, J. R.; Richards, R. L. Recent Advances in the Chemistry of Nitrogen Fixation. *Chem. Rev.* **1978**, *78*, 589–625.

(71) Yandulov, D. V.; Schrock, R. R. Catalytic Reduction of Dinitrogen to Ammonia at a Single Molybdenum Center. *Science* **2003**, *301*, 76–78.

(72) Schrock, R. R. Catalytic Reduction of Dinitrogen under Mild Conditions. *Chem. Commun.* **2003**, *3*, 2389.

(73) Arashiba, K.; Miyake, Y.; Nishibayashi, Y. A Molybdenum Complex Bearing PNP-Type Pincer Ligands Leads to the Catalytic Reduction of Dinitrogen into Ammonia. *Nat. Chem.* **2011**, *3*, 120–125.

(74) Kuriyama, S.; Arashiba, K.; Nakajima, K.; Tanaka, H.; Kamaru, N.; Yoshizawa, K.; Nishibayashi, Y. Catalytic Formation of Ammonia from Molecular Dinitrogen by Use of Dinitrogen-Bridged Dimolybdenum–Dinitrogen Complexes Bearing PNP-Pincer Ligands: Remarkable Effect of Substituent at PNP-Pincer Ligand. *J. Am. Chem. Soc.* **2014**, *136*, 9719–9731.

(75) Tanaka, H.; Arashiba, K.; Kuriyama, S.; Sasada, A.; Nakajima, K.; Yoshizawa, K.; Nishibayashi, Y. Unique Behaviour of Dinitrogen-Bridged Dimolybdenum Complexes Bearing Pincer Ligand towards Catalytic Formation of Ammonia. *Nat. Commun.* **2014**, *5*, 3737.

(76) Nishibayashi, Y. Recent Progress in Transition-Metal-Catalyzed Reduction of Molecular Dinitrogen under Ambient Reaction Conditions. *Inorg. Chem.* **2015**, *54*, 9234–9247.

(77) Arashiba, K.; Kinoshita, E.; Kuriyama, S.; Eizawa, A.; Nakajima, K.; Tanaka, H.; Yoshizawa, K.; Nishibayashi, Y. Catalytic Reduction of Dinitrogen to Ammonia by Use of Molybdenum–Nitride Complexes Bearing a Tridentate Triphosphine as Catalysts. *J. Am. Chem. Soc.* **2015**, *137*, 5666–5669.

(78) Tanaka, H.; Nishibayashi, Y.; Yoshizawa, K. Interplay between Theory and Experiment for Ammonia Synthesis Catalyzed by Transition Metal Complexes. *Acc. Chem. Res.* **2016**, *49*, 987–995.

(79) Anderson, J. S.; Rittle, J.; Peters, J. C. Catalytic Conversion of Nitrogen to Ammonia by an Iron Model Complex. *Nature* **2013**, *501*, 84–87.

(80) Creutz, S. E.; Peters, J. C. Catalytic Reduction of N_2 to NH_3 by an Fe-N_2 Complex Featuring a C-Atom Anchor. *J. Am. Chem. Soc.* **2014**, *136*, 1105–1115.

(81) Anderson, J. S.; Cutsail, G. E.; Rittle, J.; Connor, B. A.; Gunderson, W. A.; Zhang, L.; Hoffman, B. M.; Peters, J. C. Characterization of an Fe≡N–NH_2 Intermediate Relevant to Catalytic N_2 Reduction to NH_3. *J. Am. Chem. Soc.* **2015**, *137*, 7803–7809.

(82) Laplaza, C. E.; Cummins, C. C. Dinitrogen Cleavage by a Three-Coordinate Molybdenum(III) Complex. *Science* **1995**, *268*, 861–863.

(83) Shima, T.; Hu, S.; Luo, G.; Kang, X.; Luo, Y.; Hou, Z. Dinitrogen Cleavage and Hydrogenation by a Trinuclear Titanium Polyhydride Complex. *Science* **2013**, *340*, 1549–1552.

(84) Doyle, L. R.; Wooles, A. J.; Liddle, S. T. Bimetallic Cooperative Cleavage of Dinitrogen to Nitride and Tandem Frustrated Lewis Pair Hydrogenation to Ammonia. *Angew. Chem. Int. Ed.* **2019**, *58*, 6674–6677.

(85) Spencer, L. P.; MacKay, B. A.; Patrick, B. O.; Fryzuk, M. D. Inner-Sphere Two-Electron Reduction Leads to Cleavage and Functionalization of Coordinated Dinitrogen. *Proc. Natl. Acad. Sci.* **2006**, *103*, 17094–17098.

(86) Semproni, S. P.; Chirik, P. J. Synthesis of a Base-Free Hafnium Nitride from N_2 Cleavage: A Versatile Platform for Dinitrogen Functionalization. *J. Am. Chem. Soc.* **2013**, *135*, 11373–11383.

(87) Clentsmith, G. K. B.; Bates, V. M. E.; Hitchcock, P. B.; Cloke, F. G. N. Reductive Cleavage of Dinitrogen by a Vanadium Diamidoamine Complex: The Molecular Structures of $[V(Me_3SiN\{CH_2CH_2NSiMe_3\}_2)(\mu\text{-}N)]_2$ and K[V(Me$_3$SiN{CH$_2$CH$_2$NSiMe. *J. Am. Chem. Soc.* **1999**, *121*, 10444–10445.

(88) Caselli, A.; Solari, E.; Scopelliti, R.; Floriani, C.; Re, N.; Rizzoli, C.; Chiesi-Villa, A. Dinitrogen Rearranging over a Metal−Oxo Surface and Cleaving to Nitride: From the End-On to the Side-On Bonding Mode, to the Stepwise Cleavage of the N⁝N Bonds Assisted by Nb^{III}-Calix[4]Arene. *J. Am. Chem. Soc.* **2000**, *122*, 3652–3670.

(89) Kawaguchi, H.; Matsuo, T. Dinitrogen-Bond Cleavage in a Niobium Complex Supported by a Tridentate Aryloxide Ligand. *Angew. Chem. Int. Ed.* **2002**, *41*, 2792–2794.

(90) Rodriguez, M. M.; Bill, E.; Brennessel, W. W.; Holland, P. L. N_2 Reduction and Hydrogenation to Ammonia by a Molecular Iron-Potassium Complex. *Science* **2011**, *334*, 780–783.

(91) Solari, E.; Da Silva, C.; Iacono, B.; Hesschenbrouck, J.; Rizzoli, C.; Scopelliti, R.; Floriani, C. Photochemical Activation of the N≡N Bond in a Dimolybdenum-Dinitrogen Complex: Formation of a Molybdenum Nitride. *Angew. Chem.* **2001**, *113*, 4025–4027.

(92) Hebden, T. J.; Schrock, R. R.; Takase, M. K.; Mueller, P.; Muller, P.; Müller, P. Cleavage of Dinitrogen to Yield a (t-BuPOCOP)Molybdenum(IV) Nitride. *Chem. Commun.* **2012**, *48*, 1851–1853.

(93) Miyazaki, T.; Tanaka, H.; Tanabe, Y.; Yuki, M.; Nakajima, K.; Yoshizawa, K.; Nishibayashi, Y. Cleavage and Formation of Molecular Dinitrogen in a Single System Assisted by Molybdenum Complexes Bearing Ferrocenyldiphosphine. *Angew. Chem. Int. Ed.* **2014**, *53*, 11488–11492.

(94) Arashiba, K.; Eizawa, A.; Tanaka, H.; Nakajima, K.; Yoshizawa, K.; Nishibayashi, Y. Catalytic Nitrogen Fixation via Direct Cleavage of Nitrogen–Nitrogen Triple Bond of Molecular Dinitrogen under Ambient Reaction Conditions. *Bull. Chem. Soc. Jpn.* **2017**, *90*, 1111–1118.

(95) Silantyev, G. A.; Förster, M.; Schluschaß, B.; Abbenseth, J.; Würtele, C.; Volkmann, C.; Holthausen, M. C.; Schneider, S. Dinitrogen Splitting Coupled to Protonation. *Angew. Chem. Int. Ed.* **2017**, *56*, 5872–5876.

(96) Itabashi, T.; Mori, I.; Arashiba, K.; Eizawa, A.; Nakajima, K.; Nishibayashi, Y. Effect of Substituents on Molybdenum Triiodide Complexes Bearing PNP-Type Pincer Ligands toward Catalytic Nitrogen Fixation. *Dalton Trans.* **2019**, *48*, 3182–3186.

(97) Ashida, Y.; Arashiba, K.; Nakajima, K.; Nishibayashi, Y. Molybdenum-Catalysed Ammonia Production with Samarium Diiodide and Alcohols or Water. *Nature* **2019**, *568*, 536–540.

(98) Katayama, A.; Ohta, T.; Wasada-Tsutsui, Y.; Inomata, T.; Ozawa, T.; Ogura, T.; Masuda, H. Dinitrogen-Molybdenum Complex Induces Dinitrogen Cleavage by One-Electron Oxidation. *Angew. Chem. Int. Ed.* **2019**, *58*, 11279–11284.

(99) Singh, D.; Buratto, W. R.; Torres, J. F.; Murray, L. J. Activation of Dinitrogen by Polynuclear Metal Complexes. *Chem. Rev.* **2020**, *120*, 5517–5581.

(100) Eizawa, A.; Arashiba, K.; Egi, A.; Tanaka, H.; Nakajima, K.; Yoshizawa, K.; Nishibayashi, Y. Catalytic Reactivity of Molybdenum–Trihalide Complexes Bearing PCP-Type Pincer Ligands. *Chem. Asian J.* **2019**, *14*, 2091–2096.

(101) Ashida, Y.; Kondo, S.; Arashiba, K.; Kikuchi, T.; Nakajima, K.; Kakimoto, S.; Nishibayashi, Y. A Practical Synthesis of Ammonia from Nitrogen Gas, Samarium Diiodide and Water Catalyzed by a Molybdenum–PCP Pincer Complex. *Synthesis* **2019**, *51*, 3792–3795.

(102) Elgrishi, N.; Rountree, K. J.; McCarthy, B. D.; Rountree, E. S.; Eisenhart, T. T.; Dempsey, J. L. A Practical Beginner's Guide to Cyclic Voltammetry. *J. Chem. Educ.* **2018**, *95*, 197–206.

(103) Savéant, J.-M. Molecular Catalysis of Electrochemical Reactions. Mechanistic Aspects. *Chem. Rev.* **2008**, *108*, 2348–2378.

(104) Gritzner, G.; Kuta, J. Recommendations on Reporting Electrode Potentials in Nonaqueous Solvents (Recommendations 1983). *Pure Appl. Chem.* **1984**, *56*, 461–466.

(105) Connelly, N. G.; Geiger, W. E. Chemical Redox Agents for Organometallic Chemistry. *Chem. Rev.* **1996**, *96*, 877–910.

(106) Al-Salih, T. I.; Pickett, C. J. Electron-Transfer Reactions in Nitrogen Fixation. Part 1. The Electrosynthesis of Dinitrogen, Hydride, Isocyanide, and Carbonyl Complexes of Molybdenum: Intermediates, Mechanisms, and Energetics. *J. Chem. Soc. Dalton Trans.* **1985**, *53*, 1255.

(107) Hughes, D. L.; Mohammed, M. Y.; Pickett, C. J. Electroreduction of Co-Ordinated Cyanide to the Aminocarbyne Ligand (CNH_2) and a Pathway for Isomerisation of Ligating Methyleneamide (NCH_2): Reactions at Molybdenum of Relevance to Cyanide Reduction by Nitrogenase. *J. Chem. Soc. Chem. Commun.* **1989**, 1399.

(108) Whited, M. T.; Mankad, N. P.; Lee, Y.; Oblad, P. F.; Peters, J. C. Dinitrogen Complexes Supported by Tris(Phosphino)Silyl Ligands. *Inorg. Chem.* **2009**, *48*, 2507–2517.

(109) Mankad, N. P.; Whited, M. T.; Peters, J. C. Terminal Fe^{I}–N_2 and Fe^{II}···H–C Interactions Supported by Tris(Phosphino)Silyl Ligands. *Angew. Chem. Int. Ed.* **2007**, *46*, 5768–5771.

(110) Moret, M.-E.; Peters, J. C. Terminal Iron Dinitrogen and Iron Imide Complexes Supported by a Tris(Phosphino)Borane Ligand. *Angew. Chem. Int. Ed.* **2011**, *50*, 2063–2067.

(111) Anderson, J. S.; Moret, M. E.; Peters, J. C. Conversion of Fe-NH_2 to Fe-N_2 with Release of NH_3. *J. Am. Chem. Soc.* **2013**, *135*, 534–537.

(112) Del Castillo, T. J.; Thompson, N. B.; Peters, J. C. A Synthetic Single-Site Fe Nitrogenase: High Turnover, Freeze-Quench 57Fe Mössbauer Data, and a Hydride Resting State. *J. Am. Chem. Soc.* **2016**, *138*, 5341–5350.

(113) Clouston, L. J.; Bernales, V.; Carlson, R. K.; Gagliardi, L.; Lu, C. C. Bimetallic Cobalt-

Dinitrogen Complexes: Impact of the Supporting Metal on N_2 Activation. *Inorg. Chem.* **2015**, *54*, 9263–9270.

(114) Peters, J. C.; Cherry, J.-P. F.; Thomas, J. C.; Baraldo, L.; Mindiola, D. J.; Davis, W. M.; Cummins, C. C. Redox-Catalyzed Binding of Dinitrogen by Molybdenum N-Tert-Hydrocarbylanilide Complexes: Implications for Dinitrogen Functionalization and Reductive Cleavage. **1999**.

(115) Rittle, J.; McCrory, C. C. L.; Peters, J. C. A 10^6-Fold Enhancement in N_2-Binding Affinity of an $Fe_2(\mu\text{-}H)_2$ Core upon Reduction to a Mixed-Valence $Fe^{II}Fe^{I}$ State. *J. Am. Chem. Soc.* **2014**, *136*, 13853–13862.

(116) Prokopchuk, D. E.; Wiedner, E. S.; Walter, E. D.; Popescu, C. V.; Piro, N. A.; Kassel, W. S.; Bullock, R. M.; Mock, M. T. Catalytic N_2 Reduction to Silylamines and Thermodynamics of N_2 Binding at Square Planar Fe. *J. Am. Chem. Soc.* **2017**, *139*, 9291–9301.

(117) Klopsch, I.; Finger, M.; Würtele, C.; Milde, B.; Werz, D. B.; Schneider, S. Dinitrogen Splitting and Functionalization in the Coordination Sphere of Rhenium. *J. Am. Chem. Soc.* **2014**, *136*, 6881–6883.

(118) Lindley, B. M.; van Alten, R. S.; Finger, M.; Schendzielorz, F.; Würtele, C.; Miller, A. J. M.; Siewert, I.; Schneider, S. Mechanism of Chemical and Electrochemical N_2 Splitting by a Rhenium Pincer Complex. *J. Am. Chem. Soc.* **2018**, *140*, 7922–7935.

(119) Kätelhön, E.; Compton, R. G. Testing and Validating Electroanalytical Simulations. *Analyst* **2015**, *140*, 2592–2598.

(120) Richard G. Compton, E. L. K. R. W. Understanding voltammetry : simulation of electrode processes; London : Imperial College Press, [2014], 2014.

(121) van Alten, R. S.; Wätjen, F.; Demeshko, S.; Miller, A. J. M.; Würtele, C.; Siewert, I.; Schneider, S. (Electro-)Chemical Splitting of Dinitrogen with a Rhenium Pincer Complex. *Eur. J. Inorg. Chem.* **2020**, *2020*, 1402–1410.

(122) Bruch, Q. J.; Lindley, B. M.; Askevold, B.; Schneider, S.; Miller, A. J. M. A Ruthenium Hydrido Dinitrogen Core Conserved across Multielectron/Multiproton Changes to the Pincer Ligand Backbone. *Inorg. Chem.* **2018**, *57*, 1964–1975.

(123) Schendzielorz, F.; Finger, M.; Abbenseth, J.; Würtele, C.; Krewald, V.; Schneider, S. Metal-Ligand Cooperative Synthesis of Benzonitrile by Electrochemical Reduction and Photolytic Splitting of Dinitrogen. *Angew. Chem. Int. Ed.* **2019**, *58*, 830–834.

(124) Bruch, Q. J.; Connor, G. P.; Chen, C.-H.; Holland, P. L.; Mayer, J. M.; Hasanayn, F.; Miller, A. J. M. Dinitrogen Reduction to Ammonium at Rhenium Utilizing Light and Proton-Coupled Electron Transfer. *J. Am. Chem. Soc.* **2019**, *141*, 20198–20208.

(125) Falivene, L.; Cao, Z.; Petta, A.; Serra, L.; Poater, A.; Oliva, R.; Scarano, V.; Cavallo, L. Towards the Online Computer-Aided Design of Catalytic Pockets. *Nat. Chem.* **2019**, *11*, 872–879.

(126) Howell, J. A. S.; Burkinshaw, P. M. Ligand Substitution Reactions at Low-Valent Four-,

Five-, and Six-Coordinate Transition Metal Centers. *Chem. Rev.* **1983**, *83*, 557–599.

(127) Richens, D. T. Ligand Substitution Reactions at Inorganic Centers. *Chem. Rev.* **2005**, *105*, 1961–2002.

(128) Yandulov, D. V.; Schrock, R. R. Studies Relevant to Catalytic Reduction of Dinitrogen to Ammonia by Molybdenum Triamidoamine Complexes. *Inorg. Chem.* **2005**, *44*, 1103–1117.

(129) Faggion, D.; Gonçalves, W. D. G.; Dupont, J. CO_2 Electroreduction in Ionic Liquids. *Front. Chem.* **2019**, *7*, 1–8.

(130) Aurbach, D.; Talyosef, Y.; Markovsky, B.; Markevich, E.; Zinigrad, E.; Asraf, L.; Gnanaraj, J. S.; Kim, H.-J. Design of Electrolyte Solutions for Li and Li-Ion Batteries: A Review. *Electrochim. Acta* **2004**, *50*, 247–254.

(131) Stoian, S. A.; Vela, J.; Smith, J. M.; Sadique, A. R.; Holland, P. L.; Münck, E.; Bominaar, E. L. Mössbauer and Computational Study of an N_2-Bridged Diiron Diketiminate Complex: Parallel Alignment of the Iron Spins by Direct Antiferromagnetic Exchange with Activated Dinitrogen. *J. Am. Chem. Soc.* **2006**, *128*, 10181–10192.

(132) Smith, J. M.; Sadique, A. R.; Cundari, T. R.; Rodgers, K. R.; Lukat-Rodgers, G.; Lachicotte, R. J.; Flaschenriem, C. J.; Vela, J.; Holland, P. L. Studies of Low-Coordinate Iron Dinitrogen Complexes. *J. Am. Chem. Soc.* **2006**, *128*, 756–769.

(133) Holland, P. L. Metal-Dioxygen and Metal-Dinitrogen Complexes: Where Are the Electrons? *Dalton Trans.* **2010**, *39*, 5415–5425.

(134) Connor, G. P.; Holland, P. L. Coordination Chemistry Insights into the Role of Alkali Metal Promoters in Dinitrogen Reduction. *Catal. Today* **2017**, *286*, 21–40.

(135) Bhutto, S. M.; Holland, P. L. Dinitrogen Activation and Functionalization Using β-Diketiminate Iron Complexes. *Eur. J. Inorg. Chem.* **2019**, *2019*, 1861–1869.

(136) Chatt, J.; Fay, R. C.; Richards, R. L. Preparation and Characterisation of the Dinuclear Dinitrogen Complex, Trichloro-μ-Dinitrogen-Bis(Tetrahydrofuran){chlorotetrakis[Dimethyl-(Phenyl)Phosphine]Rhenium(I)}chromium(III). *J. Chem. Soc. A* **1971**, 702–704.

(137) Woen, D. H.; Chen, G. P.; Ziller, J. W.; Boyle, T. J.; Furche, F.; Evans, W. J. End-On Bridging Dinitrogen Complex of Scandium. *J. Am. Chem. Soc.* **2017**, *139*, 14861–14864.

(138) Curley, J. J.; Cook, T. R.; Reece, S. Y.; Müller, P.; Cummins, C. C. Shining Light on Dinitrogen Cleavage: Structural Features, Redox Chemistry, and Photochemistry of the Key Intermediate Bridging Dinitrogen Complex. *J. Am. Chem. Soc.* **2008**, *130*, 9394–9405.

(139) Laplaza, C. E.; Johnson, M. J. A.; Peters, J. C.; Odom, A. L.; Kim, E.; Cummins, C. C.; George, G. N.; Pickering, I. J. Dinitrogen Cleavage by Three-Coordinate Molybdenum(III) Complexes: Mechanistic and Structural Data. *J. Am. Chem. Soc.* **1996**, *118*, 8623–8638.

(140) Harrison, D. F.; Weissberger, E.; Taube, H. Binuclear Ion Containing Nitrogen as a Bridging Group. *Science* **1968**, *159*, 320–322.

(141) Ghosh, R.; Kanzelberger, M.; Emge, T. J.; Hall, G. S.; Goldman, A. S. Dinitrogen Complexes of Pincer-Ligated Iridium. *Organometallics* **2006**, *25*, 5668–5671.

(142) Rittle, J.; Peters, J. C. Fe-N_2/CO Complexes That Model a Possible Role for the Interstitial C Atom of FeMo-Cofactor (FeMoco). *Proc. Natl. Acad. Sci.* **2013**, *110*, 15898–15903.

(143) Klopsch, I.; Yuzik-Klimova, E. Y.; Schneider, S. Functionalization of N_2 by Mid to Late Transition Metals via N–N Bond Cleavage; Nishibayashi, Y., Ed.; Springer: Cham, 2017; pp 71–112.

(144) Treitel, I. M.; Flood, M. T.; Marsh, R. E.; Gray, H. B. Molecular and Electronic Structure of M-Nitrogen-Decaamminediruthenium(II). *J. Am. Chem. Soc.* **1969**, *91*, 6512–6513.

(145) Cui, Q.; Musaev, D. G.; Svensson, M.; Sieber, S.; Morokuma, K. N_2 Cleavage by Three-Coordinate Group 6 Complexes. W(III) Complexes Would Be Better Than Mo(III) Complexes. *J. Am. Chem. Soc.* **1995**, *117*, 12366–12367.

(146) Neyman, K. M.; Nasluzov, V. A.; Hahn, J.; Landis, C. R.; Rösch, N. Density Functional Study of N 2 Activation by Molybdenum(III) Complexes. Unusually Strong Relativistic Effects in 4d Metal Compounds. *Organometallics* **1997**, *16*, 995–1000.

(147) Cherry, J.-P. F.; Johnson, A. R.; Baraldo, L. M.; Tsai, Y.-C.; Cummins, C. C.; Kryatov, S. V.; Rybak-Akimova, E. V.; Capps, K. B.; Hoff, C. D.; Haar, C. M.; Nolan, S. P. On the Origin of Selective Nitrous Oxide N−N Bond Cleavage by Three-Coordinate Molybdenum(III) Complexes. *J. Am. Chem. Soc.* **2001**, *123*, 7271–7286.

(148) Mindiola, D. J.; Meyer, K.; Cherry, J.-P. F.; Baker, T. A.; Cummins, C. C. Dinitrogen Cleavage Stemming from a Heterodinuclear Niobium/Molybdenum N_2 Complex: New Nitridoniobium Systems Including a Niobazene Cyclic Trimer. *Organometallics* **2000**, *19*, 1622–1624.

(149) Liao, Q.; Cavaillé, A.; Saffon-Merceron, N.; Mézailles, N. Direct Synthesis of Silylamine from N_2 and a Silane: Mediated by a Tridentate Phosphine Molybdenum Fragment. *Angew. Chem. Int. Ed.* **2016**, *55*, 11212–11216.

(150) Shih, K.-Y.; Schrock, R. R.; Kempe, R. Synthesis of Molybdenum Complexes That Contain Silylated Triamidoamine Ligands. A μ-Dinitrogen Complex, Methyl and Acetylide Complexes, and Coupling of Acetylides. *J. Am. Chem. Soc.* **1994**, *116*, 8804–8805.

(151) Chisholm, M. H.; Cotton, F. A.; Frenz, B. A.; Reichert, W. W.; Shive, L. W.; Stults, B. R. The Molybdenum-Molybdenum Triple Bond. 1. Hexakis(Dimethylamido)Dimolybdenum and Some Homologues: Preparation, Structure, and Properties. *J. Am. Chem. Soc.* **1976**, *98*, 4469–4476.

(152) Geoffroy, G. L.; Wrighton, M. S. Organometallic photochemistry; Academic Pr, 1979.

(153) Huss, A. S.; Curley, J. J.; Cummins, C. C.; Blank, D. A. Relaxation and Dissociation Following Photoexcitation of the (μ-N_2)[Mo(N[t-Bu]Ar) $_3$]$_2$ Dinitrogen Cleavage

Intermediate. *J. Phys. Chem. B* **2013**, *117*, 1429–1436.

(154) Rafiq, S.; Bezdek, M. J.; Koch, M.; Chirik, P. J.; Scholes, G. D. Ultrafast Photophysics of a Dinitrogen-Bridged Molybdenum Complex. *J. Am. Chem. Soc.* **2018**, *140*, 6298–6307.

(155) Rafiq, S.; Bezdek, M. J.; Chirik, P. J.; Scholes, G. D. Dinitrogen Coupling to a Terpyridine-Molybdenum Chromophore Is Switched on by Fermi Resonance. *Chem* **2019**, *5*, 402–416.

(156) Burgess Jr., D. R. NIST Chemistry WebBook, NIST Standard Reference Database Number 69. In *NIST Chemistry WebBook*; Linstrom, P. J., Mallard, W. G., Eds.; National Institute of Standards and Technology: Gaithersburg, MD, 2017; p 20899.

(157) Ware, D. C.; Taube, H. Substitution-Induced N-N Coupling for Nitride Coordinated to Osmium(VI). *Inorg. Chem.* **1991**, *30*, 4605–4610.

(158) Seymore, S. B.; Brown, S. N. Polar Effects in Nitride Coupling Reactions. *Inorg. Chem.* **2002**, *41*, 462–469.

(159) Berry, J. F. Terminal Nitrido and Imido Complexes of the Late Transition Metals. *Comments Inorg. Chem.* **2009**, *30*, 28–66.

(160) Smith, J. M. Reactive Transition Metal Nitride Complexes. In *Prog. Inorg. Chem.*; John Wiley & Sons, Inc., 2014; Vol. 58, pp 417–470.

(161) Dehnicke, K.; Strähle, J. The Transition Metal-Nitrogen Multiple Bond. *Angew. Chem. Int. Ed.* **1981**, *20*, 413–426.

(162) Dehnicke, K.; Strähle, J. Nitrido Complexes of Transition Metals. *Angew. Chem. Int. Ed.* **1992**, *31*, 955–978.

(163) Man, W.-L.; Lam, W. W. Y.; Lau, T.-C. Reactivity of Nitrido Complexes of Ruthenium(VI), Osmium(VI), and Manganese(V) Bearing Schiff Base and Simple Anionic Ligands. *Acc. Chem. Res.* **2014**, *47*, 427–439.

(164) Eikey, R. A.; Abu-Omar, M. M. Nitrido and Imido Transition Metal Complexes of Groups 6-8. *Coord. Chem. Rev.* **2003**, *243*, 83–124.

(165) Curley, J. J.; Sceats, E. L.; Cummins, C. C. A Cycle for Organic Nitrile Synthesis via Dinitrogen Cleavage. *J. Am. Chem. Soc.* **2006**, *128*, 14036–14037.

(166) Abbenseth, J.; Finger, M.; Würtele, C.; Kasanmascheff, M.; Schneider, S. Coupling of Terminal Iridium Nitrido Complexes. *Inorg. Chem. Front.* **2016**, *3*, 469–477.

(167) Keener, M.; Peterson, M.; Hernández Sánchez, R.; Oswald, V. F.; Wu, G.; Ménard, G. Towards Catalytic Ammonia Oxidation to Dinitrogen: A Synthetic Cycle by Using a Simple Manganese Complex. *Chem. Eur. J.* **2017**, *23*, 11479–11484.

(168) Connor, G. P.; Mercado, B. Q.; Lant, H. M. C.; Mayer, J. M.; Holland, P. L. Chemical Oxidation of a Coordinated PNP-Pincer Ligand Forms Unexpected Re-Nitroxide Complexes with Reversal of Nitride Reactivity. *Inorg. Chem.* **2019**, *58*, 10791–10801.

(169) Klopsch, I.; Schendzielorz, F.; Volkmann, C.; Würtele, C.; Schneider, S. Synthesis of

Benzonitrile from Dinitrogen. *Z. Anorg. Allg. Chemie* **2018**, *644*, 916–919.

(170) Lindley, B. M.; Bruch, Q. J.; White, P. S.; Hasanayn, F.; Miller, A. J. M. Ammonia Synthesis from a Pincer Ruthenium Nitride via Metal–Ligand Cooperative Proton-Coupled Electron Transfer. *J. Am. Chem. Soc.* **2017**, *139*, 5305–5308.

(171) Darcy, J. W.; Koronkiewicz, B.; Parada, G. A.; Mayer, J. M. A Continuum of Proton-Coupled Electron Transfer Reactivity. *Acc. Chem. Res.* **2018**, *51*, 2391–2399.

(172) Waidmann, C. R.; Miller, A. J. M.; Ng, C.-W. A.; Scheuermann, M. L.; Porter, T. R.; Tronic, T. A.; Mayer, J. M. Using Combinations of Oxidants and Bases as PCET Reactants: Thermochemical and Practical Considerations. *Energy Environ. Sci.* **2012**, *5*, 7771–7780.

(173) Bezdek, M. J.; Guo, S.; Chirik, P. J. Coordination-Induced Weakening of Ammonia, Water, and Hydrazine X–H Bonds in a Molybdenum Complex. *Science* **2016**, *354*, 730–733.

(174) Bezdek, M. J.; Pappas, I.; Chirik, P. J. Determining and Understanding N-H Bond Strengths in Synthetic Nitrogen Fixation Cycles. In *Nitrogen Fixation*; Nishibayashi, Y., Ed.; Springer International Publishing: Cham, 2017; pp 1–21.

(175) Wang, D.; Loose, F.; Chirik, P. J.; Knowles, R. R. N–H Bond Formation in a Manganese(V) Nitride Yields Ammonia by Light-Driven Proton-Coupled Electron Transfer. *J. Am. Chem. Soc.* **2019**, *141*, 4795–4799.

(176) Matson, B. D.; Peters, J. C. Fe-Mediated HER vs N_2RR: Exploring Factors That Contribute to Selectivity in $P_3^EFe(N_2)$ (E = B, Si, C) Catalyst Model Systems. *ACS Catal.* **2018**, *8*, 1448–1455.

(177) Huynh, M. T.; Anson, C. W.; Cavell, A. C.; Stahl, S. S.; Hammes-Schiffer, S. Quinone 1 e^- and 2 e^-/2 H^+ Reduction Potentials: Identification and Analysis of Deviations from Systematic Scaling Relationships. *J. Am. Chem. Soc.* **2016**, *138*, 15903–15910.

(178) Chalkley, M. J.; Del Castillo, T. J.; Matson, B. D.; Roddy, J. P.; Peters, J. C. Catalytic N_2-to-NH_3 Conversion by Fe at Lower Driving Force: A Proposed Role for Metallocene-Mediated PCET. *ACS Cent. Sci.* **2017**, *3*, 217–223.

(179) Chalkley, M. J.; Oyala, P. H.; Peters, J. C. Cp* Noninnocence Leads to a Remarkably Weak C–H Bond via Metallocene Protonation. *J. Am. Chem. Soc.* **2019**, *141*, 4721–4729.

(180) Cheng, J.-P.; Lu, Y.; Zhu, X.-Q.; Sun, Y.; Bi, F.; He, J. Heterolytic and Homolytic N−H Bond Dissociation Energies of 4-Substituted Hantzsch 2,6-Dimethyl-1,4-Dihydropyridines and the Effect of One-Electron Transfer on the N−H Bond Activation. *J. Org. Chem.* **2000**, *65*, 3853–3857.

(181) Kamochi, Y.; Kudo, T. Novel Reduction of Carboxylic Acids, Esters, Amides and Nitriles Using Samarium Diiodide in the Presence of Water. *Chem. Lett.* **1993**, *22*, 1495–1498.

(182) Chciuk, T. V.; Anderson, W. R.; Flowers, R. A. Proton-Coupled Electron Transfer in the Reduction of Carbonyls by Samarium Diiodide–Water Complexes. *J. Am. Chem. Soc.* **2016**, *138*, 8738–8741.

(183) Kolmar, S. S.; Mayer, J. M. $SmI_2(H_2O)_n$ Reduction of Electron Rich Enamines by Proton-Coupled Electron Transfer. *J. Am. Chem. Soc.* **2017**, *139*, 10687–10692.

(184) Chciuk, T. V.; Anderson, W. R.; Flowers, R. A. Interplay between Substrate and Proton Donor Coordination in Reductions of Carbonyls by SmI_2–Water Through Proton-Coupled Electron-Transfer. *J. Am. Chem. Soc.* **2018**, *140*, 15342–15352.

(185) Margulieux, G. W.; Bezdek, M. J.; Turner, Z. R.; Chirik, P. J. Ammonia Activation, H_2 Evolution and Nitride Formation from a Molybdenum Complex with a Chemically and Redox Noninnocent Ligand. *J. Am. Chem. Soc.* **2017**, *139*, 6110–6113.

(186) Loose, F.; Wang, D.; Tian, L.; Scholes, G. D.; Knowles, R. R.; Chirik, P. J. Evaluation of Excited State Bond Weakening for Ammonia Synthesis from a Manganese Nitride: Stepwise Proton Coupled Electron Transfer Is Preferred over Hydrogen Atom Transfer. *Chem. Commun.* **2019**, *55*, 5595–5598.

(187) Weinberg, D. R.; Gagliardi, C. J.; Hull, J. F.; Murphy, C. F.; Kent, C. A.; Westlake, B. C.; Paul, A.; Ess, D. H.; McCafferty, D. G.; Meyer, T. J. Proton-Coupled Electron Transfer. *Chem. Rev.* **2012**, *112*, 4016–4093.

(188) Costentin, C.; Robert, M.; Savéant, J.-M. Update 1 of: Electrochemical Approach to the Mechanistic Study of Proton-Coupled Electron Transfer. *Chem. Rev.* **2010**, *110*, PR1–PR40.

(189) Nutting, J. E.; Rafiee, M.; Stahl, S. S. Tetramethylpiperidine N -Oxyl (TEMPO), Phthalimide N -Oxyl (PINO), and Related N -Oxyl Species: Electrochemical Properties and Their Use in Electrocatalytic Reactions. *Chem. Rev.* **2018**, *118*, 4834–4885.

(190) Francke, R.; Little, R. D. Redox Catalysis in Organic Electrosynthesis: Basic Principles and Recent Developments. *Chem. Soc. Rev.* **2014**, *43*, 2492.

(191) Greenlee, L. F.; Renner, J. N.; Foster, S. L. The Use of Controls for Consistent and Accurate Measurements of Electrocatalytic Ammonia Synthesis from Dinitrogen. *ACS Catal.* **2018**, *8*, 7820–7827.

(192) Tang, C.; Qiao, S.-Z. How to Explore Ambient Electrocatalytic Nitrogen Reduction Reliably and Insightfully. *Chem. Soc. Rev.* **2019**, *48*, 3166–3180.

(193) Kibsgaard, J.; Nørskov, J. K.; Chorkendorff, I. The Difficulty of Proving Electrochemical Ammonia Synthesis. *ACS Energy Lett.* **2019**, *4*, 2986–2988.

(194) Suryanto, B. H. R.; Du, H. L.; Wang, D.; Chen, J.; Simonov, A. N.; MacFarlane, D. R. Challenges and Prospects in the Catalysis of Electroreduction of Nitrogen to Ammonia. *Nat. Catal.* **2019**, *2*, 290–296.

(195) Andersen, S. Z.; Čolić, V.; Yang, S.; Schwalbe, J. A.; Nielander, A. C.; McEnaney, J. M.; Enemark-Rasmussen, K.; Baker, J. G.; Singh, A. R.; Rohr, B. A.; Statt, M. J.; Blair, S. J.; Mezzavilla, S.; Kibsgaard, J.; Vesborg, P. C. K. K.; Cargnello, M.; Bent, S. F.; Jaramillo, T. F.; Stephens, I. E. L. L.; Nørskov, J. K.; Chorkendorff, I. A Rigorous Electrochemical Ammonia Synthesis Protocol with Quantitative Isotope Measurements. *Nature* **2019**, *570*, 504–508.

(196) Duan, G. Y.; Ren, Y.; Tang, Y.; Sun, Y. Z.; Chen, Y. M.; Wan, P. Y.; Yang, X. J. Improving the Reliability and Accuracy of Ammonia Quantification in Electro- and Photochemical Synthesis. *ChemSusChem* **2020**, *13*, 88–96.